

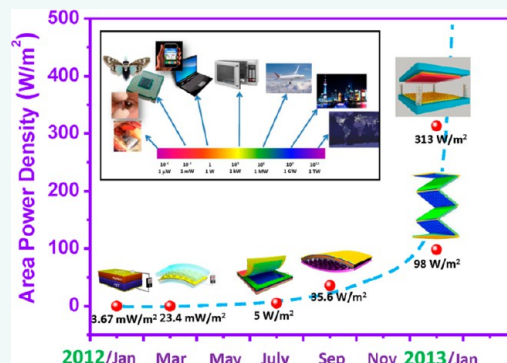
# Triboelectric Nanogenerators as New Energy Technology for Self-Powered Systems and as Active Mechanical and Chemical Sensors

Zhong Lin Wang<sup>†,‡,\*</sup>

<sup>†</sup>School of Materials Science and Engineering, Georgia Institute of Technology, Atlanta, Georgia 30332-0245, United States and <sup>‡</sup>Beijing Institute of Nanoenergy and Nanosystems, Chinese Academy of Sciences, Beijing, China

This Review is contributed by a recipient of the 2013 ACS Nano Lectureship Awards, presented at the International Conference on Nanoscience & Technology, China 2013 (ChinaNANO 2013) in September 2013. The ACS Nano Lectureship honors the contributions of scientists whose work has significantly impacted the fields of nanoscience and nanotechnology.

**ABSTRACT** Triboelectrification is an effect that is known to each and every one probably since ancient Greek time, but it is usually taken as a negative effect and is avoided in many technologies. We have recently invented a triboelectric nanogenerator (TENG) that is used to convert mechanical energy into electricity by a conjunction of triboelectrification and electrostatic induction. As for this power generation unit, in the inner circuit, a potential is created by the triboelectric effect due to the charge transfer between two thin organic/inorganic films that exhibit opposite tribo-polarity; in the outer circuit, electrons are driven to flow between two electrodes attached on the back sides of the films in order to balance the potential. Since the most useful materials for TENG are organic, it is also named organic nanogenerator, which is the first using organic materials for harvesting mechanical energy. In this paper, we review the fundamentals of the TENG in the three basic operation modes: vertical contact-separation mode, in-plane sliding mode, and single-electrode mode. Ever since the first report of the TENG in January 2012, the output power density of TENG has been improved 5 orders of magnitude within 12 months. The area power density reaches  $313 \text{ W/m}^2$ , volume density reaches  $490 \text{ kW/m}^3$ , and a conversion efficiency of  $\sim 60\%$  has been demonstrated. The TENG can be applied to harvest all kinds of mechanical energy that is available but wasted in our daily life, such as human motion, walking, vibration, mechanical triggering, rotating tire, wind, flowing water, and more. Alternatively, TENG can also be used as a self-powered sensor for actively detecting the static and dynamic processes arising from mechanical agitation using the voltage and current output signals of the TENG, respectively, with potential applications for touch pad and smart skin technologies. To enhance the performance of the TENG, besides the vast choices of materials in the triboelectric series, from polymer to metal and to fabric, the morphologies of their surfaces can be modified by physical techniques with the creation of pyramid-, square-, or hemisphere-based micro- or nanopatterns, which are effective for enhancing the contact area and possibly the triboelectrification. The surfaces of the materials can be functionalized chemically using various molecules, nanotubes, nanowires, or nanoparticles, in order to enhance the triboelectric effect. The contact materials can be composites, such as embedding nanoparticles in a polymer matrix, which may change not only the surface electrification but also the permittivity of the materials so that they can be effective for electrostatic induction. Therefore, there are numerous ways to enhance the performance of the TENG from the materials point of view. This gives an excellent opportunity for chemists and materials scientists to do extensive study both in the basic science and in practical applications. We anticipate that a better enhancement of the output power density will be achieved in the next few years. The TENG is possible not only for self-powered portable electronics but also as a new energy technology with potential to contribute to the world energy in the near future.



**KEYWORDS:** triboelectrification · triboelectric nanogenerator · self-powered system · active sensor · organic nanogenerator

The massive development of the world electronic technology follows a general trend of miniaturization, portability, and functionality. The development of computers is a typical example of miniaturization, from the vacuum-tube-based huge-sized machine to solid-state MOSFET-based mainframe computers and later laptop

computers. The tremendous increase of popularity of handheld cell phones is a typical example of portable/mobile electronics. The next few decades will be about building functionality on existing electronics, which inevitably involves developing a range of sensors including but not limited to navigation, motion, chemical, biological,

\* Address correspondence to [zlwang@gatech.edu](mailto:zlwang@gatech.edu).

Received for review September 3, 2013 and accepted September 30, 2013.

Published online September 30, 2013  
10.1021/nn404614z

© 2013 American Chemical Society

and gas sensors. The near future development is about electronics that are much smaller than the size of a cell phone, so that each person on average can have at least dozens to hundreds of such small electronics. Such small-sized electronics operate at ultralow power consumption, making it possible to be powered by the energy harvested from our living environment.<sup>1</sup> It will become impractical if sensor networks have to be powered entirely by batteries because of the huge number of devices, large scope of distribution, and difficulty to track and recycle to minimize environmental impact and possibly health hazards. Therefore, power sources are desperately needed for independent and continuous operations of such small electronics, which could be used widely for ultrasensitive chemical and bimolecular sensors, nanorobotics, microelectromechanical systems, remote and mobile environmental sensors, homeland security, and even portable/wearable personal electronics.

New technologies that can harvest energy from the environment as sustainable self-sufficient micro/nano-power sources are newly emerging fields of nano-energy, which is about the applications of nano-materials and nanotechnology for harvesting energy for powering micro/nanosystems. In the last 8 years, we have been developing nanogenerators (NGs) for building self-powered systems and as active sensors. We have mainly utilized two physics effects for harvesting small-magnitude mechanical energies: piezoelectric effect and triboelectric effect. A basic introduction about piezoelectric NG has been given in a recent book<sup>2</sup> and a few review articles.<sup>3,4</sup> The objective of this paper is to give a summary about the fundamentals of the triboelectric nanogenerator (TENG), which is a device that converts mechanical energy into electricity using the coupling effects between triboelectrification and electrostatic induction through the contact-separation or relative sliding between two materials that have opposite tribo-polarity and its updated progress and potential applications as a new energy technology and as self-powered active sensors.

**Fundamentals of Triboelectrification.** The triboelectric effect is a contact-induced electrification in which a material becomes electrically charged after it is contacted with a different material through friction. Triboelectric effect is a general cause of every day's electrostatics. The sign of the charges to be carried by a material depends on its relative polarity in comparison to the material to which it will contact.

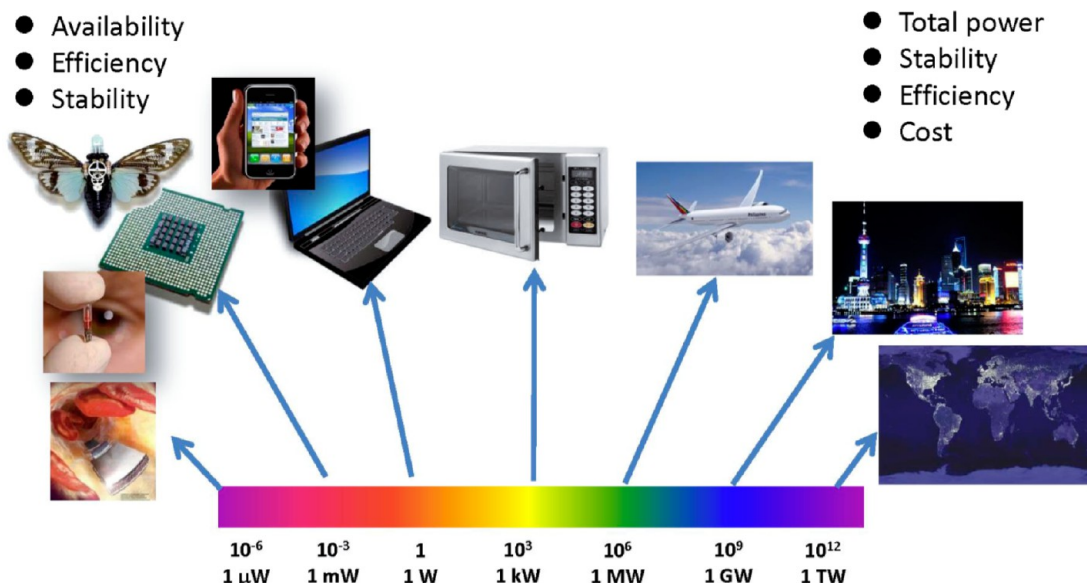
Triboelectric effect is probably one of a few effects that have been known for thousands of years. Although this is one of the most frequently experienced effects that each and every one of us inevitably uses every day, the mechanism behind triboelectrification is still being studied possibly with debate.<sup>5,6</sup> It is generally believed that, after two different materials come into contact, a chemical bond is formed between some parts of the

**GLOSSARY:** **triboelectric effect** - a contact-induced electrification in which a material becomes electrically charged after it is contacted with a different material through friction; **nanoenergy** - the applications of nano-materials and nanotechnology for harvesting energy for powering micro/nanosystems; **triboelectric nanogenerator (TENG)** - a device that converts mechanical energy into electricity using the coupling effects between triboelectrification and electrostatic induction through the contact-separation or relative sliding between two materials that have opposite tribo-polarity; **self-powered active strain/force sensors** - a sensor that operates using the electric signal generated by itself in responding to mechanical triggering or agitation without applying an external power source; **PMMA** - polymethyl methacrylate; **PDMS** - polydimethylsiloxane;

two surfaces, called adhesion, and charges move from one material to the other to equalize their electrochemical potential. The transferred charges can be electrons or may be ions/molecules. When separated, some of the bonded atoms have a tendency to keep extra electrons and some a tendency to give them away, possibly producing triboelectric charges on surfaces. The objective of our study is not to investigate the mechanism of the triboelectrification, instead, use it for positive purposes.

Materials that usually have strong triboelectrification effect are likely less conductive or insulators, thus, they usually capture the transferred charges and retain them for an extended period of time, building up the electrostatic charges, which are usually considered to be a negative effect in our daily life and technology developments. We can use the following examples to illustrate the damages that can be caused by triboelectrification. Aircraft flying will develop static charges from air friction on the airframe, which will interfere with radio frequency communication. Electrostatic charges are an important concern for safety, due to the fact that it can cause explosion and ignite flammable vapors. Carts/cars that may carry volatile liquids, flammable gases, or explosive chemicals have to be discharged properly to avoid fire. Some electronic devices, most notably CMOS-integrated circuits and MOSFET transistors, can be accidentally destroyed by high-voltage static discharge that may be carried by gloves. Therefore, triboelectrification is mostly taken as a negative effect in our daily life, industrial manufacturing, and transportation. Therefore, by surprise, although triboelectrification has been known for thousands of years, it has not been used for many positive applications. In this paper, we give a review on a new, innovative, and important application of triboelectric effect for converting mechanical energy into electricity and as self-powered active mechanical sensors.

**Nanoscale Energy (Nanoenergy) and Macroscale Energy.** In general, energy usually means the power required to



### Nanoenergy: energy required for the sustainable, maintenance-free and self-powered operation of micro/nano-systems

Figure 1. Magnitude of power and its corresponding applications. Macroscale energy is for powering a city and even a country; nanoscale energy is to power tiny small electronics. Both applications are measured by different characteristics.

run a factory, a city, or a country. This is generally referred to as macroscale energy, which is measured in the scale of gigawatt or megawatt. General characteristics of a technology for macroscale energy are the total power output, stability, conversion efficiency, and cost. In many cases, cost is the most important measure, such as for solar cells (Figure 1).

On the other hand, with the tremendous increase in the number of portable electronics, developing energy-storage-related technologies is vitally important because most are run by batteries. Although the power consumption of each is rather small, the total number of devices is extremely huge. Over three billion people around the world have cell phones. With the implementation of sensor networks around the globe, a gigantic number of sensors will be distributed worldwide; powering of such a horrendous network consisting of trillions of sensors would be impossible using batteries because one has to find the location, replace batteries, and inspect the proper operation of batteries from time to time. Energy harvesting from the environment in which the sensor is employed is a possible solution. This is the field of nanoenergy, which is the power for sustainable, maintenance-free, and self-powered operation of micro/nanosystems.<sup>7</sup> The general characteristics for nanoenergy power sources are availability, efficiency, and stability (Figure 1). In a case where a device is used under the light, the use of solar energy would be a natural choice. In a case of a device used near an engine possibly in the dark, harvesting mechanical vibration energy would be the best choice. As for biological application, harvesting deformation

energy from muscle stretching would be a good approach. Although we may have a super high efficient solar cell, the condition under which the device will work may have little light, the highly efficient solar cell is not the choice for this device. Therefore, the type of energy to be harvested depends on the working environment of the device. This is what we mean by the availability of the energy source for a particular application. The stability of the energy source is also important because it guarantees the long-term operation of the device. Take solar cells as an example; it has strong dependence on the day or night, weather, or even season. This is the reason that we have been developing technologies for converting mechanical energy into electricity for self-powered sensors.

**Traditional Triboelectric Generators.** Traditional triboelectric generator is a mechanical device that produces static electricity or electricity at high voltage by contact charging. The most popular ones are the Wimshurst machine and Van de Graaff generator, which were invented in ~1880 and 1929, respectively. Both machines use the accumulated static charges generated by triboelectrification; the tribo-charges are transferred from a rotating belt to a metal brush by the corona discharging (e.g., the electric-field-induced arching of air); once the accumulated charge density reaches a critical value, discharging over two opposite electrodes occurs (Figure 2). It appears that the traditional triboelectric generator is a high voltage source, and there is no current unless there is a discharging.

**Triboelectric Nanogenerators.** Although the triboelectrification effect has been known for thousands of

years, a fundamental understanding about it is rather limited. Research has been conducted to characterize the triboelectrification process using various methods such as rolling sphere tool-collecting-induced charges from rolling spheres on top of a dielectric disk<sup>8,9</sup> and using atomic force microscopy (AFM) to measure surface electrostatic force or potential on surfaces contacted by micropatterned materials.<sup>10–12</sup> However,

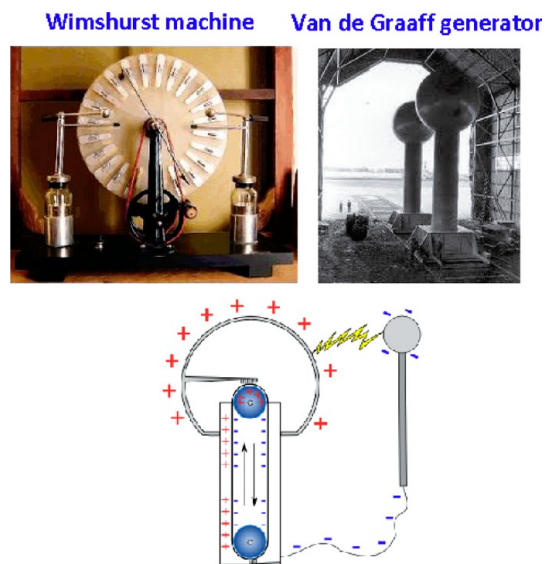


**Figure 2.** Wimshurst machine and Van de Graaff generator, developed a century ago, are the only two possible applications of triboelectrification related to energy.

these methods either lack an accurate control of the electrification process and/or cannot directly reveal the triboelectric interface, thus hardly achieving a quantitative understanding about the *in situ* triboelectric process.

We have demonstrated an *in situ* method to quantitatively characterize the triboelectrification at the nanoscale *via* a combination of contact-mode AFM and scanning Kelvin probe microscopy.<sup>13</sup> As a benefit of the capability of controlled charge transferring and *in situ* measurement, AFM can be used to investigate the triboelectric charge transfer at surfaces. As a model system, a SiO<sub>2</sub> thin film was rubbed for multiple cycles at the same area with constant contact force. The corresponding scanning Kelvin probe microscopy images after each friction cycle are shown in Figure 3a, and the extracted potential profiles are presented in Figure 3b. Within eight cycles of friction, the magnitude of the potential increased from 0.1 to 0.7 V at a slowing rate. As shown in Figure 3c, there is a clear trend for the surface charge accumulation and saturation process. By quantitatively fitting the experimental data, surface charge density before the triboelectric process is  $\sigma_0 = (-12 \pm 3) \mu\text{C/m}^2$ , and saturation charge density after infinite numbers of cycles of friction is  $\sigma_\infty = (-150 \pm 8) \mu\text{C/m}^2$ . The electric field at the vicinity of the surface is  $\sim 1.7 \times 10^7 \text{ V/m}$ , which can easily generate a high voltage. The contact-induced charge transfer is the experimental base of our TENG.

**Vertical Contact-Separation Mode-Based TENG: Dielectric-to-Dielectric Case.** The discovery of TENG

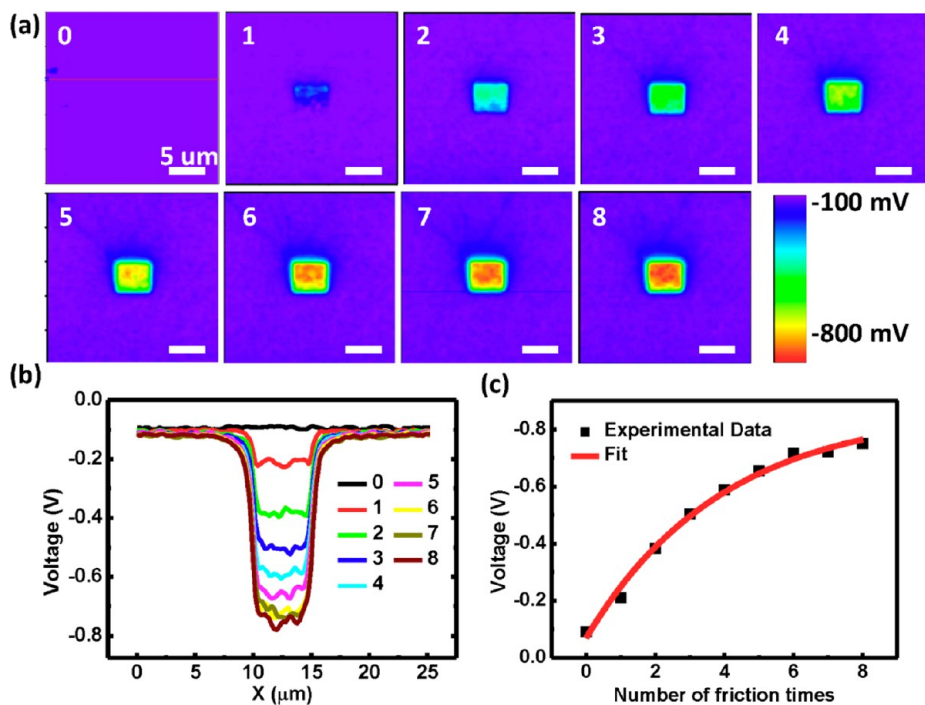


**Figure 3.** Triboelectric charge accumulation on the SiO<sub>2</sub> surface with the increase of the number of repeated rubbings at the same area. (a) Series of surface potential images taken in the same area from intact status to the one after the 8th rubbing cycles, and (b) their corresponding potential profiles. (c) Derived surface potential as a function of the number of friction cycles and the simulation based on charge accumulation theory. Reproduced from ref 13. Copyright 2013 American Chemical Society.

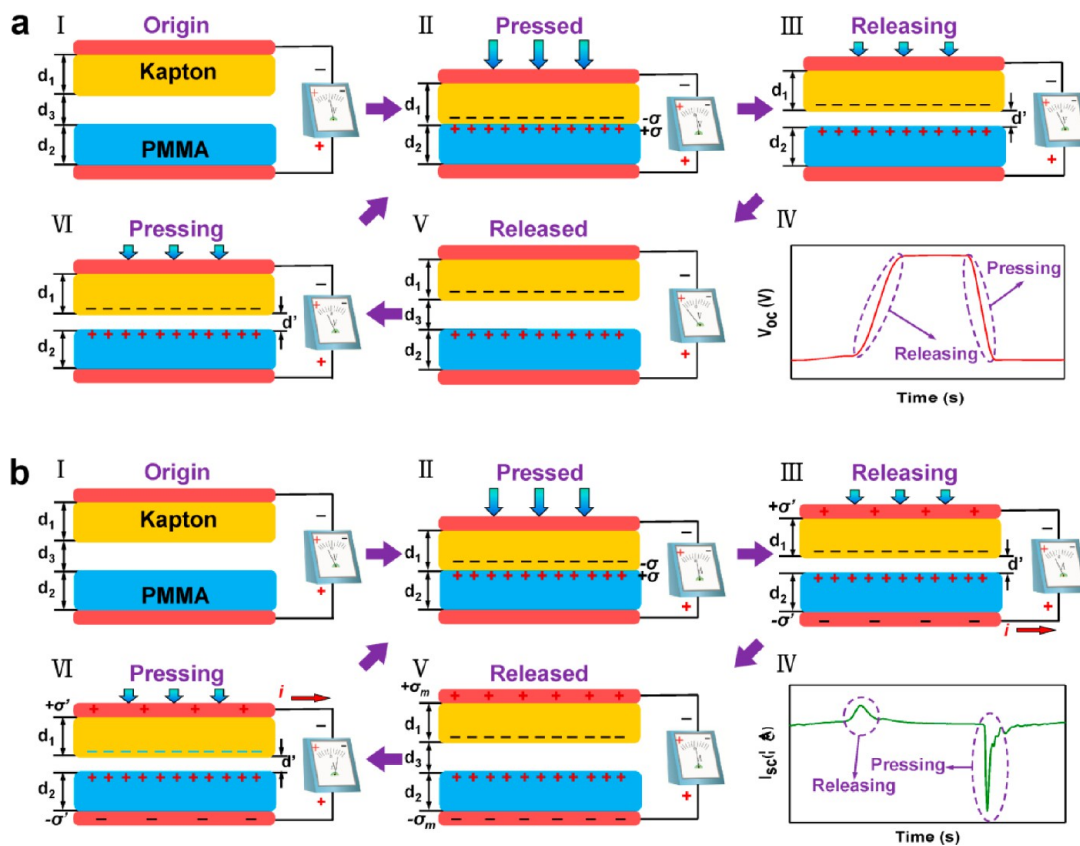


**Figure 4.** Sketch that illustrates the operating principle of the TENG for dielectric-to-dielectric in contact-separation mode. (a) Open-circuit condition. (b) Short-circuit condition. The polymer nanowires are not shown for the purpose of simplification. Reproduced from ref 16. Copyright 2012 American Chemical Society.

can be traced back to our development of piezoelectric nanogenerators,<sup>1–4</sup> in which ZnO nanowires were grown on polymer surfaces. The device was usually fully packaged without gap or void. However, in a case where a device was not fully packaged so that the bottom polymer substrate and the top packaging material might have a relative sliding or contacting, a voltage of a few volts was generated. This phenomenon was first considered as an “artifact” or surface electrostatic charge and was ignored. However, in early 2012, we did a systematic study about this phenomenon and found that it was a triboelectrification-driven energy conversion process.<sup>14,15</sup> This was the birth of the TENG, which is distinctly different from the traditional Van de Graaff generator in a way that electrostatic induction is introduced for output power.

The operating principle of the TENG for the case of dielectric-to-dielectric in contact mode can be described by the coupling of contact charging and electrostatic induction.<sup>16</sup> Respectively, Figure 4a,b depicts electric output of open-circuit voltage and short-circuit current. In the original state, no charge is generated or induced, with no electric potential difference (EPD) between the two electrodes (Figure 4aI). With an externally applied force, the two polymers are brought into contact with each other. Surface charge transfer then takes place at the contact area due to triboelectrification.

According to the triboelectric series,<sup>17,18</sup> which is a list of materials based on their tendency to gain or lose charges, electrons are injected from PMMA into Kapton, resulting in net negative charges at the Kapton surface and net positive charges at the PMMA surface, respectively. It is worth noting that the insulating property of the polymers allows a long-time retention of triboelectric charges for hours or even days. Since they are only confined on the surface, charges with opposite signs coincide at almost the same plane, generating practically no EPD between the two electrodes (Figure 4aII).

As the generator starts to be released, the Kapton film tends to revert back to its original position due to its own resilience. Once the two polymers separate, an EPD is then established between the two electrodes (Figure 4aIII). If we define electric potential of the bottom electrode ( $U_{BE}$ ) to be zero, electric potential of the top electrode ( $U_{TE}$ ) can be calculated by

$$U_{TE} = -\frac{\sigma d'}{\epsilon_0} \quad (1)$$

where  $\sigma$  is the triboelectric charge density,  $\epsilon_0$  is the vacuum permittivity, and  $d'$  is the interlayer distance at a given state.

As the generator is being released,  $V_{oc}$  increases until reaching the maximum value when the Kapton

film fully reverts to the original position (Figure 4aIV and Figure 4aV). Such a signal will remain constant provided that the input impedance of the electrometer is infinitely large.

If pressing is immediately followed, the EPD starts diminishing as the two polymer layers get closer to each other. As a result,  $V_{oc}$  drops from the maximum value to zero when a full contact is made again between the two polymers (Figure 4aV,VI).

If the two electrodes are shorted, any established EPD shown in eq 1 as the two polymers separate drives electrons to flow from the top electrode (TE) to the bottom electrode (Figure 4bIII) in order to balance the generated triboelectric potential, resulting in an instantaneous positive current during the releasing process (Figure 4bIV). The net effect is that induced charges accumulate with positive sign on the top electrode and negative sign on the bottom electrode (Figure 4bV). The induced charge density ( $\sigma'$ ) when the generator is fully released is given by<sup>16</sup>

$$\sigma' = \frac{\sigma d' \epsilon_{rk} \epsilon_{rp}}{d_1 \epsilon_{rp} + d' \epsilon_{rk} \epsilon_{rp} + d_2 \epsilon_{rp}} \quad (2)$$

where  $\epsilon_{rk}$  and  $\epsilon_{rp}$  are the relative permittivity of Kapton and PMMA, respectively, and  $d_1$  and  $d_2$  are the thicknesses of the Kapton film and the PMMA layer. The maximum value of  $\sigma'_{max}$  is obtained by substituting  $d_3$  for  $d'$  in the equation above.

Once the generator is pressed again, reduction of the interlayer distance would make the top electrode possess a higher electric potential than the bottom electrode. As a consequence, electrons are driven from the bottom electrode back to the top electrode, reducing the amount of induced charges (Figure 4bVI). This process corresponds to an instantaneous negative current (Figure 4bV). When the two polymers are in contact again, all induced charges are neutralized (Figure 4bII).

Fabrication of the TENG is relatively simple, easy, low-cost, and sometimes no cleanroom equipment is even needed. The TENG has a layered structure with two substrates, as schemed at the top left of Figure 5.<sup>19</sup> Polymethyl methacrylate (PMMA) was selected as the material for substrates due to its decent strength, light weight, easy processing, and low cost. On the lower side, a layer of contact electrode is prepared. The contact electrode plays dual roles of electrode and contact surface. It consists of a gold thin film and gold nanoparticles coated on the surface. In practice, such nanoparticles can be replaced by any metallic nanoparticles. On the other side, a thin film of gold is laminated between the substrate and a layer of polydimethylsiloxane (PDMS). This electrode is termed "back electrode" for later reference. The two substrates are connected by four springs installed at the corners, leaving a narrow spacing between the contact electrode and the PDMS.

A mechanical shaker was used to apply impulse impact on the TENG. Here, the interaction force generated between the gold and the PDMS is defined as contacting force. Open-circuit voltage ( $V_{oc}$ ) and short-circuit current ( $I_{sc}$ ) were measured to characterize the TENG's electric performance. With a contacting force of 10 N, the  $V_{oc}$  and the  $I_{sc}$  are presented in Figure 5a,b, respectively. The  $V_{oc}$  switched between zero and a plateau value, respectively, corresponding to the contact position and the original position. The  $I_{sc}$  exhibits AC behavior, with an equal amount of electrons flowing in opposite directions within one cycle. The experimental data validate the working principle described in Figure 4. It is observed that the current signal for the separation process has a smaller magnitude but longer duration than that for the contact process (inset of Figure 5b). It can be explained by faster contact resulting from external impact compared to slower separation caused by restoring force of the springs. The polarity of the measured electric signals can be reversed upon switching the connection polarity between the TENG and the measurement instrument. Furthermore, the AC output could be transferred to pulse output in the same direction simply by a full-wave rectifying bridge (Figure 5c).

The NG's electric output is strongly related to the contacting force, yielding higher output with larger force. At a force as small as 10 N, the NG can still produce  $I_{sc}$  ranging from 160 to 175  $\mu$ A (Figure 5d). When the force increases to 500 N, the electric output reaches a saturated value, producing a peak  $I_{sc}$  of 1.2 mA. This result is due to increased contact area with a larger force. The two contacting surfaces are neither absolutely flat nor smooth. With a larger force, due to elastic property, the PDMS can deform and fill more vacant space, thus leading to larger contact area. As a result, the electric output increases until all the vacant space is completely filled by the PDMS, reaching a saturated limit.

Resistors were connected as external loads to further investigate the effective electric power of the TENG for driving electronics. As demonstrated in Figure 5e, the instantaneous current drops with increasing load resistance due to Ohmic loss, while the voltage builds up. Consequently, the instantaneous power output ( $W = I_{peak}^2 R$ ) reached the maximum at a load resistance of 1 M $\Omega$ . At a contacting force of 500 N, a power output of 0.42 W was achieved (Figure 5f), corresponding to a power density of 109 W/m<sup>2</sup> for one layer of TENG. If the mechanical shaker was replaced by human footfalls, which can generate a contacting force between 500 and 600 N, the maximum  $I_{sc}$  could reach up to 2 mA, which can simultaneously light up 600 LEDs (Figure 5g). It corresponded to an instantaneous current of 1.1 mA at a load of 1 M $\Omega$ , instantaneous output power of 1.2 W, and power density of 313 W/m<sup>2</sup>. The corresponding triboelectric surface charge density of 594.2  $\mu$ C/m<sup>2</sup> is demonstrated.

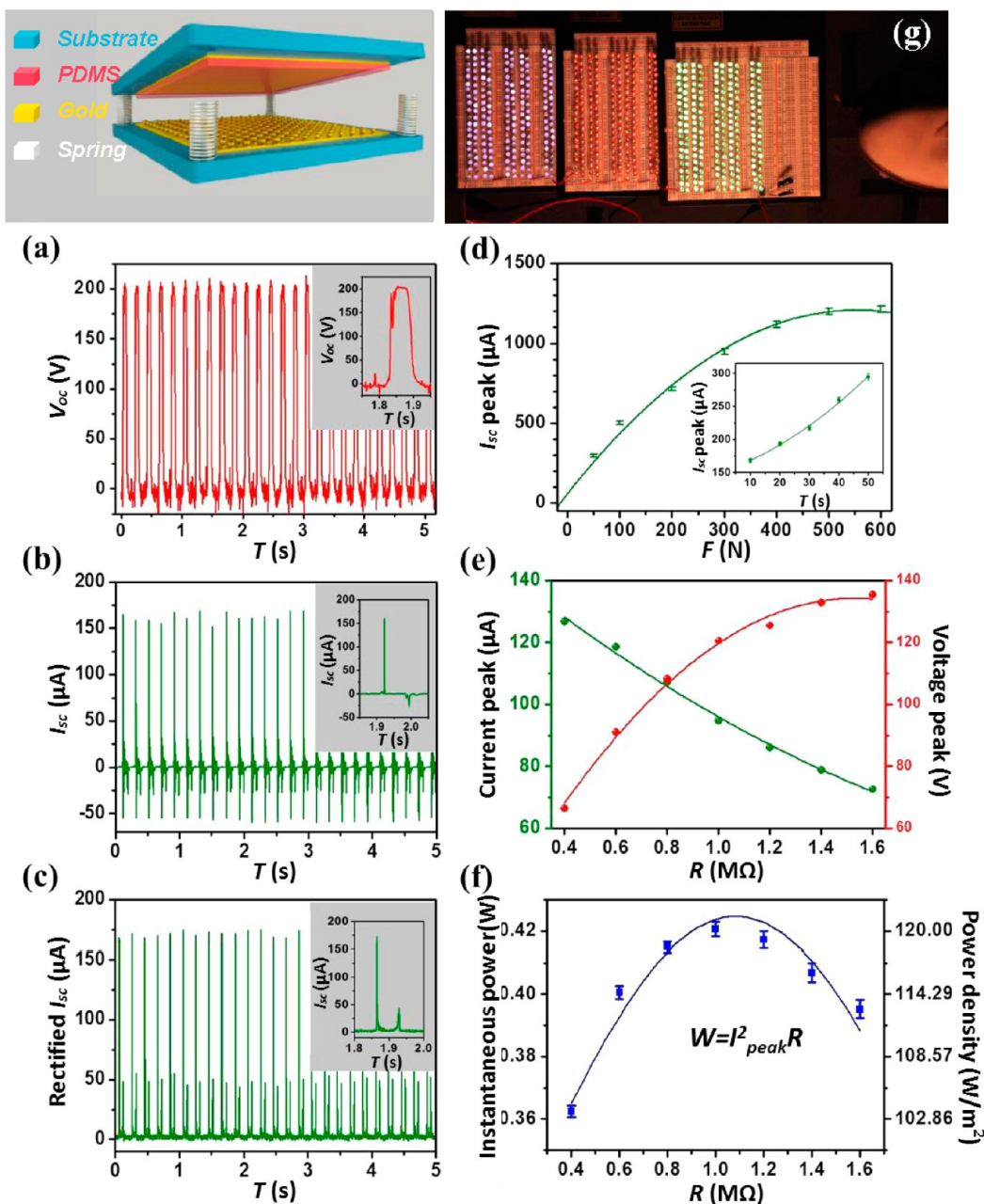


**Figure 5.** Top left: basic structure of the TENG for dielectric-to-dielectric in contact-separation mode. (a) Open-circuit voltage ( $V_{oc}$ ) at contacting force of 10 N. Inset: enlarged view of one cycle. Separation causes rising of the  $V_{oc}$  to a plateau value, and contact makes it fall back to zero. (b) Short-circuit current ( $I_{sc}$ ) at contacting force of 10 N. Inset: enlarged view of one cycle. Contact and separation correspond to a positive current pulse and a negative current pulse, respectively. (c) Rectified short-circuit current ( $I_{sc}$ ) by a full-wave bridge at contacting force of 10 N. Inset: enlarged view of one cycle, showing two current pulses in the same direction. (d) Dependence of the  $I_{sc}$  on the contacting force. Larger contacting force corresponds to higher current until saturation occurs. Inset:  $I_{sc}$  at contacting force less than 50 N. The data points represent a peak value of current pulses, while the line is the fitted result. (e) Dependence of the current output on external load resistance at a contacting force of 10 N. Increased load resistance results in lower current output but higher voltage output. The points represent the peak value of electric signals, while the line is the fitted result. (f) Dependence of the power output on external load resistance at a contacting force of 500 N, indicating maximum power output when  $R = 1 M\Omega$ . The curve is a fitted line. (g) Photograph of a setup in which the TENG acts as a direct power source for 600 commercial green, red, and blue LED bulbs, when footstep falls on the NG, simultaneously lighting up the LEDs in real-time. The estimated output open-circuit voltage is  $\sim 1200$  V. Note: all LEDs are connected serially. Reproduced from ref 20. Copyright 2013 American Chemical Society.

**Vertical Contact-Separation Mode-Based TENG: Metal-to-Dielectric Case.** The design of the TENG for the metal-to-dielectric in contact-separation mode is presented in Figure 6a.<sup>20</sup> According to the triboelectric series, electrons are injected from cellulose paper to

PTFE, resulting in net negative charges ( $Q$ ) on the PTFE surface. In a simplified model, the equivalent circuit of the TENG with an external load of  $R$  is illustrated in Figure 6b–d, in which the device can be regarded as a flat-panel capacitor. If  $\sigma$  is the charge density of the

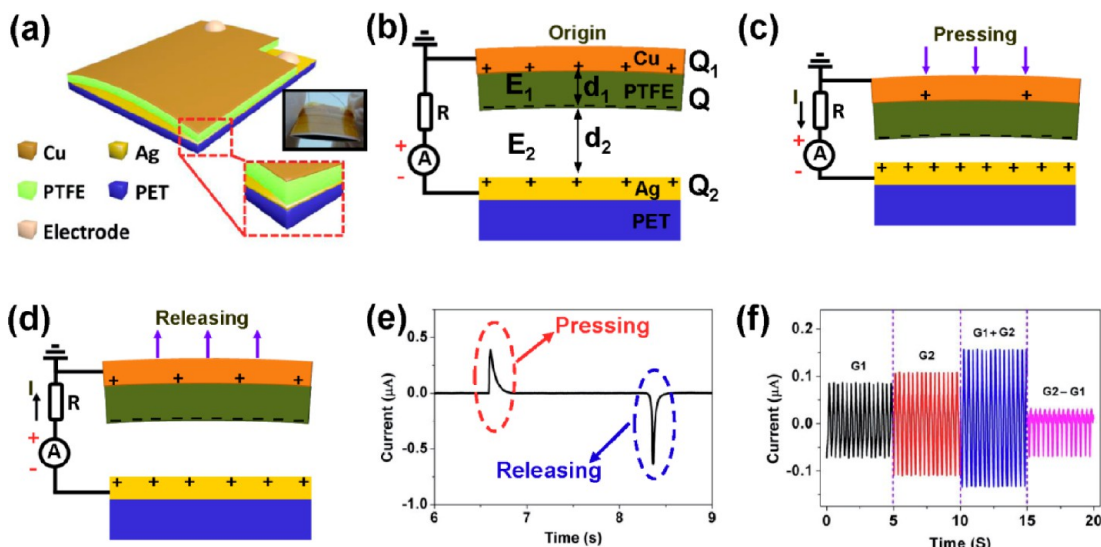


**Figure 6.** Design, operating principle, and performance of a TENG in the metal-to-dielectric in contact-separation mode. (a) Schematic diagram and digital photography of an arch-structured flexible triboelectric nanogenerator. Equivalent circuit of the TENG with an external load of  $R$  when the device is at (b) origin, (c) pressing, and (d) releasing states and (e) corresponding current–time curve, respectively. (f) Linear superposition tests of two TENGs ( $G_1$  and  $G_2$ ) connected in parallel with the same polarity ( $G_1 + G_2$ ) and opposite polarity ( $G_1 - G_2$ ). Reproduced with permission from ref 21. Copyright 2013 Elsevier.

PTFE surface,  $\sigma_1$  is the charge density of the Cu surface that is contacted with PTFE, and  $\sigma_2$  is charge density of the Ag upper surface (Figure 6b), we have<sup>21</sup>

$$\sigma_1 = -\frac{\sigma}{1 + \frac{d_1}{d_2 \epsilon_{rp}}} \quad (3)$$

$$\sigma_2 = -\sigma - \sigma_1 \quad (4)$$

where  $d_1$  and  $\epsilon_{rp}$  are the thickness and permittivity of PTFE, respectively, and charge  $Q$  is stable for a relatively long time on the PTFE surface; thus  $\sigma_1$  is dictated by the gap distance  $d_2$ . The variation of  $d_2$  will result in the redistribution of the charges between Cu and Ag electrodes through the load  $R$  that generates a current through the load, so that mechanical energy is converted into electricity. The working mechanism of the TENG is similar to a variable-capacitance generator<sup>22</sup> except that the charges are self-generated triboelectric charges rather than an external power source. Once the TENG was pressed (Figure 6c), a reduction of the interlayer distance of  $d_2$  would decrease  $\sigma_1$  according to eq 3, which results in an instantaneous positive current (Figure 6e). Upon the TENG being released (Figure 6d), the device would revert back to its original arch shape due to resilience, the interlayer distance  $d_2$  would increase, and the surface charge  $\sigma_1$  increased as well, resulting in an instantaneous negative current (Figure 6e).

Although the mechanism illustrated in Figure 6 is for a flat surface, micro- or nanopatterns can be generated on surfaces to enhance the contact area and the effectiveness of the triboelectrification. The TENG shown in Figure 7 is based on the contact

electrification between patterned PDMS as the top plate and patterned Al foil as the bottom plate (Figure 7a).<sup>18</sup> According to the triboelectric series, the purposely chosen PDMS and Al are almost at the two ends with very large differences in the ability to attract and retain electrons. The unique arch-shaped structure of the TENG from the naturally bent top plate, which helps to carry out the action of effective charge separation and contact using the elasticity of the film, is achieved by the following innovative fabrication process (Figure 7b,c): The top part starts from a piece of flat Kapton film (Figure 7b,i). A layer of 500 nm SiO<sub>2</sub> film is deposited using plasma-enhanced chemical vapor deposition (PECVD) at 250 °C (Figure 7b,ii). Upon cooling to room temperature, the Kapton will shrink to a much larger extent than the SiO<sub>2</sub> film because of the large difference in thermal expansion coefficients, so that thermal stress across the interface will make the plate bent naturally toward the SiO<sub>2</sub> side. Then, the prefabricated PDMS film with pyramid patterns is glued to the inner surface through a thin PDMS bonding layer (Figure 7b,iii). Finally, the electrode is deposited on top (Figure 7b,iv). As for the bottom plate, an aluminum foil (Figure 7c,i) is patterned with a typical photolithography process: defining the photoresist to the array of square windows (Figure 7c,ii), depositing a layer of aluminum on top (Figure 7c,iii), and finally lift-off, leaving the patterned Al cubes on the foil (Figure 7c,iv). At last, the two as-fabricated plates of the same size are attached face-to-face and sealed at the two ends. The soft Al plate will be forced to bend outward under the contraction from the other plate, so that a gap will form naturally between. The patterned surfaces of PDMS film (Figure 7d) and Al foil

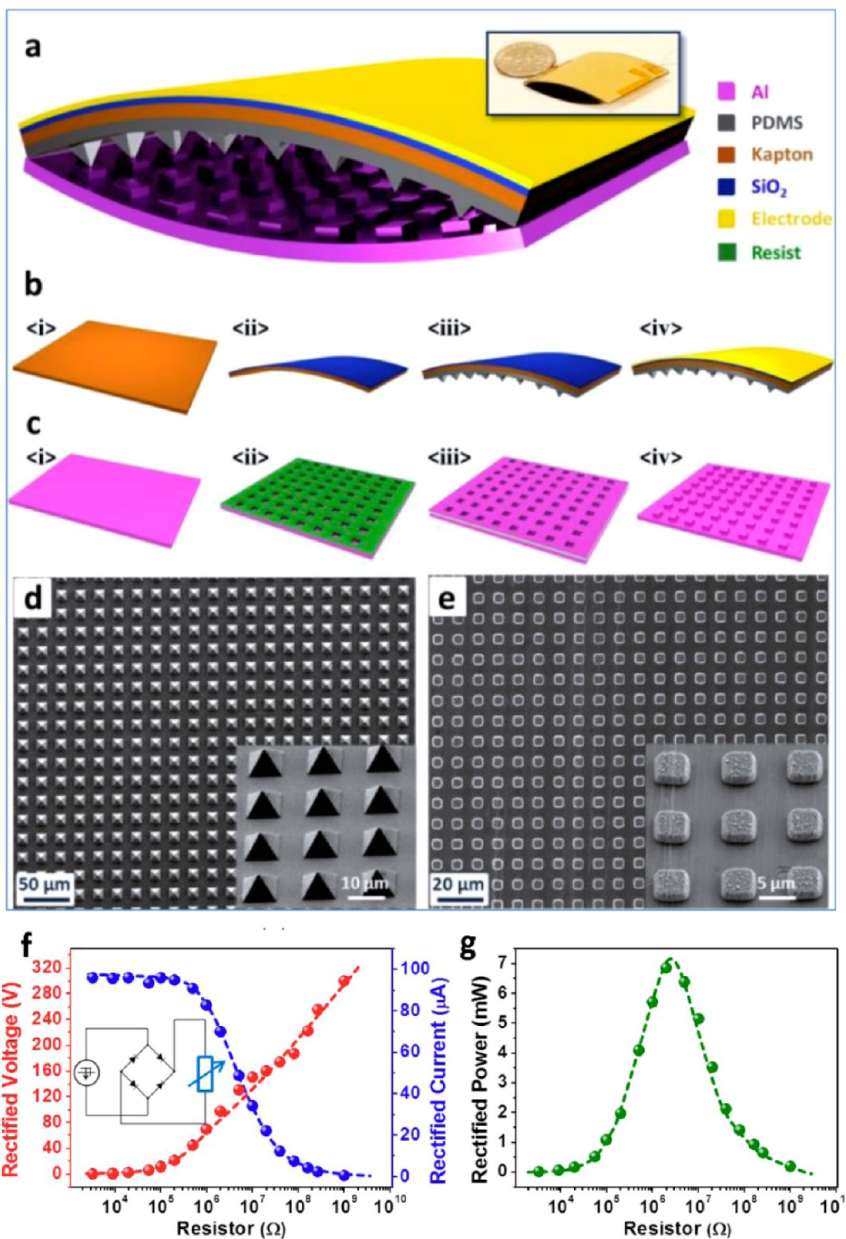


**Figure 7. Structure and fabrication process of the TENG for metal-to-dielectric in contact-separation mode. (a)** Schematic diagram showing the structural design of the arch-shaped TENG; the inset is the photograph of a typical arch-shaped TENG device. **(b,c)** Fabrication flowchart for (b) top plate and (c) bottom plate of the TENG. **(d,e)** Top view SEM images of (d) PDMS surface with pyramid patterns and (e) Al surface with cubic patterns; insets are high-magnification images at a tilted angle. **(c,d)** TENG driving a load with rectification, and dependence of (c) the output voltage, current, and (d) instantaneous power on the resistance of the load. All the dots are measured values, and the solid lines are fitted curves. Reproduced from ref 19. Copyright 2012 American Chemical Society.

(Figure 7e) are fabricated to enhance the triboelectric charging.

Based on the contact-separation triboelectrification process, multilayered and stacked TENG can be fabricated in order to enhance the total output power.<sup>23,24</sup> Such designs extend TENG from a planar structure to a volume structure. In such a case, there are two parameters for characterizing the output power: surface power density and volume power density. This type of 3D-TENG has unique advantages compared to the conventional solar cell and thermoelectric energy

generator. A solar cell can only receive light from its normal direction, in which any structure beneath a certain depth of the structure is ineffective for energy conversion. A thermal electric generator is limited by the temperature drop between its two ends, and its energy harvesting efficiency may not be improved by designing a thermoelectric generator into a layered or stacked structure.

*Lateral Sliding-Mode-Based TENG: Dielectric-on-Dielectric Case.* There are two basic friction processes: normal contact and lateral sliding. We demonstrated

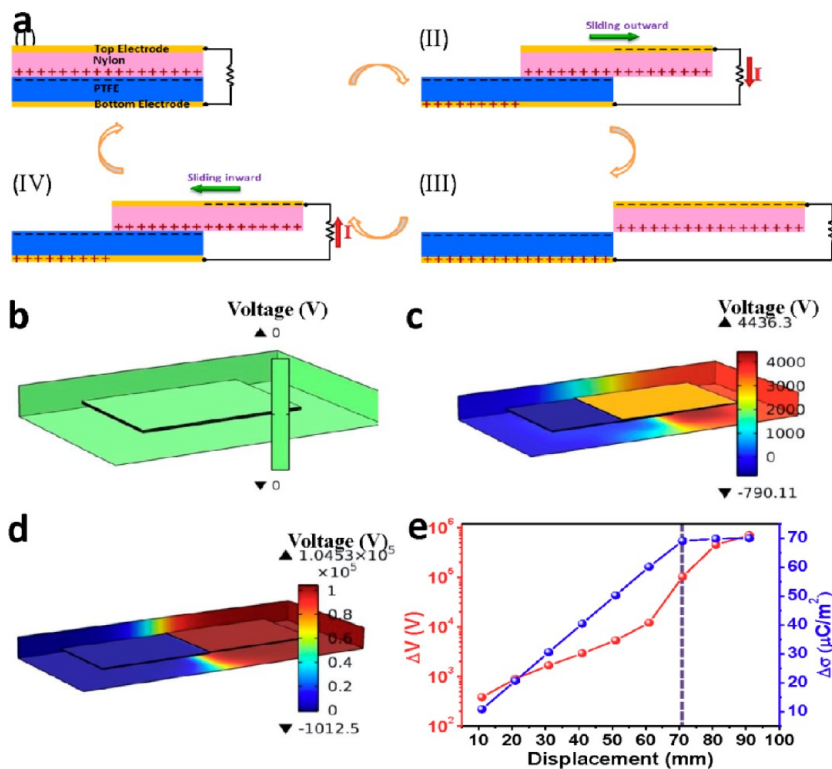


**Figure 8.** Working mechanism of the sliding mode TENG for dielectric-on-dielectric case. (a) Sketches that illustrate the electricity generation process in a full cycle of the sliding motion. (b–d) Finite element simulation of the potential difference between the two electrodes at consecutive sliding displacements: (b) 0 mm (the overlapping position); (c) 41 mm (sliding halfway out); (d) 71 mm (fully sliding out). (e) Curves of the simulated potential difference  $\Delta V$  (red) and transferred charge density  $\Delta\sigma$  (blue) vs the sliding displacement from 11 to 91 mm, in which the two plates fully slide out of each other at 71 mm (marked by the purple dot line). Reproduced from ref 26. Copyright 2013 American Chemical Society.

here a TENG that is designed based on the in-plane sliding between the two surfaces in lateral direction.<sup>25,26</sup> With an intensive triboelectrification facilitated by sliding friction, a periodic change in the contact area between two surfaces leads to a lateral separation of the charge centers, which creates a voltage drop for driving the flow of electrons in the external load. The sliding-induced electricity generation mechanism is schematically depicted in Figure 8a. In the original position (Figure 8aI), the two polymeric surfaces fully overlap and intimately contact with each other. Because of the large difference in the ability to attract electrons, the triboelectrification will leave the nylon surface with net positive charges and the PTFE with net negative charges with equal density. Since the tribo-charges on the insulators will only distribute in the surface layer and will not be leaked out for an extended period of time, the separation between the positively charged surface and negatively charged surface is negligible at this overlapping position, and thus there will be little electric potential drop across the two electrodes. Once the top plate with the positively charged surface starts to slide outward (Figure 8aII), the in-plane charge separation is initiated due to the decrease in contact surface area. The separated charges will generate an electric field pointing from the right to the left almost parallel to the plates,

inducing a higher potential at the top electrode. This potential difference will drive a current flow from the top electrode to the bottom electrode in order to generate an electric potential drop that cancels the tribo-charge-induced potential. Because the vertical distance between the electrode layer and the tribo-charged polymeric surface is negligible compared to the lateral charge separation distance, the amount of the transferred charges on the electrodes approximately equals to the amount of the separated charges at any sliding displacement. Thus, the current flow will continue with the continuation of the ongoing sliding process that keeps increasing the separated charges, until the top plate fully slides out of the bottom plate and the tribo-charged surfaces are entirely separated (Figure 8aIII). The measured current should be determined by the rate at which the two plates are being slid apart.

Subsequently, when the top plate is reverted to slide backward (Figure 8aIV), the separated charges begin to contact again but with no annihilation due to the insulator nature of the polymer materials. The redundant transferred charges on the electrodes will flow back through the external load with the increase of the contact area, in order to keep the electrostatic equilibrium. This will contribute to a current flow from the bottom electrode to the top electrode, along with the second half cycle of sliding. Once the two plates

reach the overlapping position, the charged surfaces are fully in contact again. There will be no transferred charges left on the electrode, and the device returns to the state in Figure 8a. In this entire cycle, the processes of sliding outward and inward are symmetric, so a pair of symmetric alternating current peaks should be expected.

This in-plane charge-separation-induced potential difference and charge transfer can be verified through numerical simulation using COMSOL. The model constructed here has the same structure and dimensions ( $71\text{ mm} \times 50\text{ mm}$  surface) with the real device, and those two tribo-charged surfaces are assigned with a charge density of  $\pm 70\text{ }\mu\text{C/m}^2$ . The device is in open-circuit condition, which means no electron transfer between the two electrodes. As shown by the simulation results, when the two plates are in the fully aligned stacking position, which corresponds to the state in Figure 8a, there is no potential difference generated (Figure 8b). When the top plate slides about halfway out (with a displacement of 41 mm), there will be a 2950 V potential difference between the two electrodes (Figure 8c), and this potential difference will increase to  $1.03 \times 10^5\text{ V}$  when the top plate just slides out of contact with the bottom plate (with a displacement of 71 mm) (Figure 8d). In these simulation results of Figure 8b–d, the background planes show the potential distribution in the free space of air surrounding the TENG, as a result of the in-plane charge separation. We have also simulated the voltage between the two electrodes at a series of displacements from 11 to 91 mm. As shown in Figure 8e, the voltage keeps increasing when the displacement gets larger, even after the plates slide out of each other. This is because the voltage is a path integral of the electric field along the displacement. On the other hand, the amounts of transferred charges between the two electrodes under these different displacements are also simulated by equating the potential of the electrodes at the short-circuit condition. As shown in Figure 8e, the amount of transferred charges increases linearly with the displacement before the top plate slides out of the bottom plate (with a displacement smaller than 71 mm), but different from the trend of the voltage, the amount of transferred charges will saturate at the total amount of tribo-charges on one surface after the plates have fully slid out of each other because there is no further charge separation here. So, the effective displacement region for generating electricity is between 0 and 71 mm, where the contact area of the two plates is changed during the relative sliding of the two plates.

*Lateral Sliding-Mode-Based TENG: Metal-on-Dielectric Case with Linear Grating.* In the sliding mode, introducing linear grating on the sliding surfaces is an extremely efficient means for energy harvesting. Linear grating with uniform period is fabricated on both sliding surfaces. The rows of grating units have

the same size as intervals between, with all rows being electrically connected at both ends by two buses. The grating patterns on both sliding surfaces are identical so that they can match well with each other when aligned. Although the grating design reduces the total contact area by half, thus seemingly sacrificing half of the triboelectric charges, it increases the percentage of the mismatched area to 100% for a displacement of only a grating unit length rather than the entire length of the TENG so that it dramatically increases the transport efficiency of the induced charges. Induced free electrons can be pumped back and forth between electrodes multiple times due to the grating structure, providing multifolds of output charge compared to a nongrating TENG. Every row of the grating units can be considered as a reduced-sized TENG, and it is in parallel connection with all other rows through buses. In contrast to a nongrating TENG that needs to be fully displaced in order to complete pumping of the induced charges for one time, the grating TENG only requires a displacement of a unit length to completely transport the induced charges, largely improving the energy conversion efficiency. With further displacement of another length of the unit, back flow of the induced charges can be realized. Therefore, for a one-way sliding process across the whole length of the TENG, the induced charges can be pumped for  $2N - 1$  times in total, where  $N$  is the number of grating units. If we take into account that the contacting area decreases as the two surfaces slide apart, the following equation represents the total induced charges  $Q$  that the grating TENG can provide for a single sliding across the entire length of the TENG:<sup>24</sup>

$$Q = (2q'N)N/2 \quad (5)$$

where  $q'$  is the induced charges generated from a single grating unit for a displacement of the unit length.

To demonstrate the capability of the new principle as a direct power source, a total of 80 commercial LED bulbs were utilized as operating load (Figure 9a). They were divided into two groups, which were connected to a TENG with reversed polarity in order to clearly demonstrate the AC output without rectification (Figure 9b). Shown in Figure 9a, one substrate of the TENG was fixed on a breadboard where the LEDs were installed, while the other one was attached to human fingers. As the hand swept back and forth, the sliding was realized. For a nongrating TENG, the output current it delivers to the load is displayed in Figure 9c. It is noticed that faster sweeping generates higher current peaks as compared with those from slower sweeping. Every current peak was capable of simultaneously lighting up one group of LEDs. Due to the AC output, the two LED groups were alternately lighted up, as indicated by "ON" and "OFF" states in Figure 9d. It is worth noticing that a single sliding process

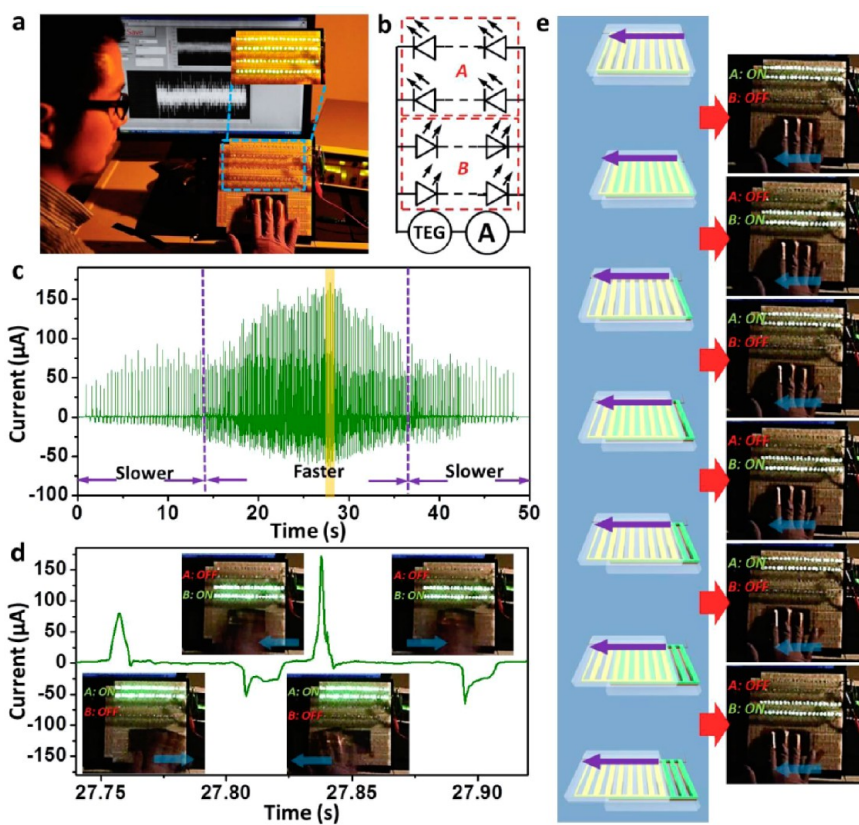


**Figure 9.** Demonstration of the sliding mode TENG for metal-on-dielectric case with a fine grating structure. (a) Photograph that shows the experimental setup. Inset: four rows of LED bulbs that are being lighted up. (b) Electric circuit diagram, indicating the four rows of LEDs are divided into two groups with reversed connection polarities. (c) Short-circuit current generated from a nongrating TENG as the relative displacement results from reciprocating sweeping of a human hand. (d) Enlarged view of the section highlighted in (c). Insets: snapshots that show the states of the two groups of LEDs corresponding to the current peaks. (e) Different stages of the sliding process as a TENG with 8 grating units is being slid apart (left column) and corresponding states of the two groups of LEDs during the sliding process (right column). Reproduced from ref 25. Copyright 2013 American Chemical Society.

corresponds to only a single current peak, which is visualized by snapshots in Figure 9d. In comparison, a grating TENG is able to power the load for multiple times within a single sliding. For a TENG with 8 grating units, only a displacement of a unit length was required to light up the LEDs. Therefore, with grating structure, not only can the TENG have substantial enhancements of current and charges but also it can provide high-frequency AC output that enables continuous operation of electric devices.

**Rotation-Mode-Based TENG.** The mechanism presented in Figure 8 can work in either one directional sliding between two plates or in rotation mode. We demonstrate a segmentally patterned disk-shaped TENG, in which a periodic overlapping and separation process of the two groups of sectors on the two concentric and closely contacted disks is achieved by relative rotation.<sup>27</sup> The basic structure of the disk TENG is composed of two disk-shaped components with four sectors each, as schematically illustrated in Figure 10a–c. The working principle of the disk TENG is based on the triboelectrification and the relative-rotation-induced cyclic in-plane charge separation between Al

and Kapton, as shown in Figure 10d. In the relative rotation, the Al surface and Kapton surface slide one relative to the other, so that the electrons will be injected from the Al foil to the inner surface of the Kapton film, leaving net positive charges on the Al foil and net negative charges on the Kapton film. The electricity generation process of the disk TENG can be divided into four stages: In stage I, the two disks are at an overlapping position. Since the two charged surfaces are closely contacted with no polarization, there will be no potential difference between the two electrodes, thus no current flow in the external load. When the Al foil rotates in reference to the Kapton film, the corresponding two segments start to have a partially mismatched contact area (stage II), and the in-plane tribo-charges are thus separated in the direction almost parallel to the sliding direction, which will induce a higher potential on the Al layer than the Kapton's electrode, thus the electrons in the electrode attached to the Kapton film will be driven to flow to the Al foil through an external load (forming a current flow in the reverse direction), so that an opposite potential is generated to balance the potential difference

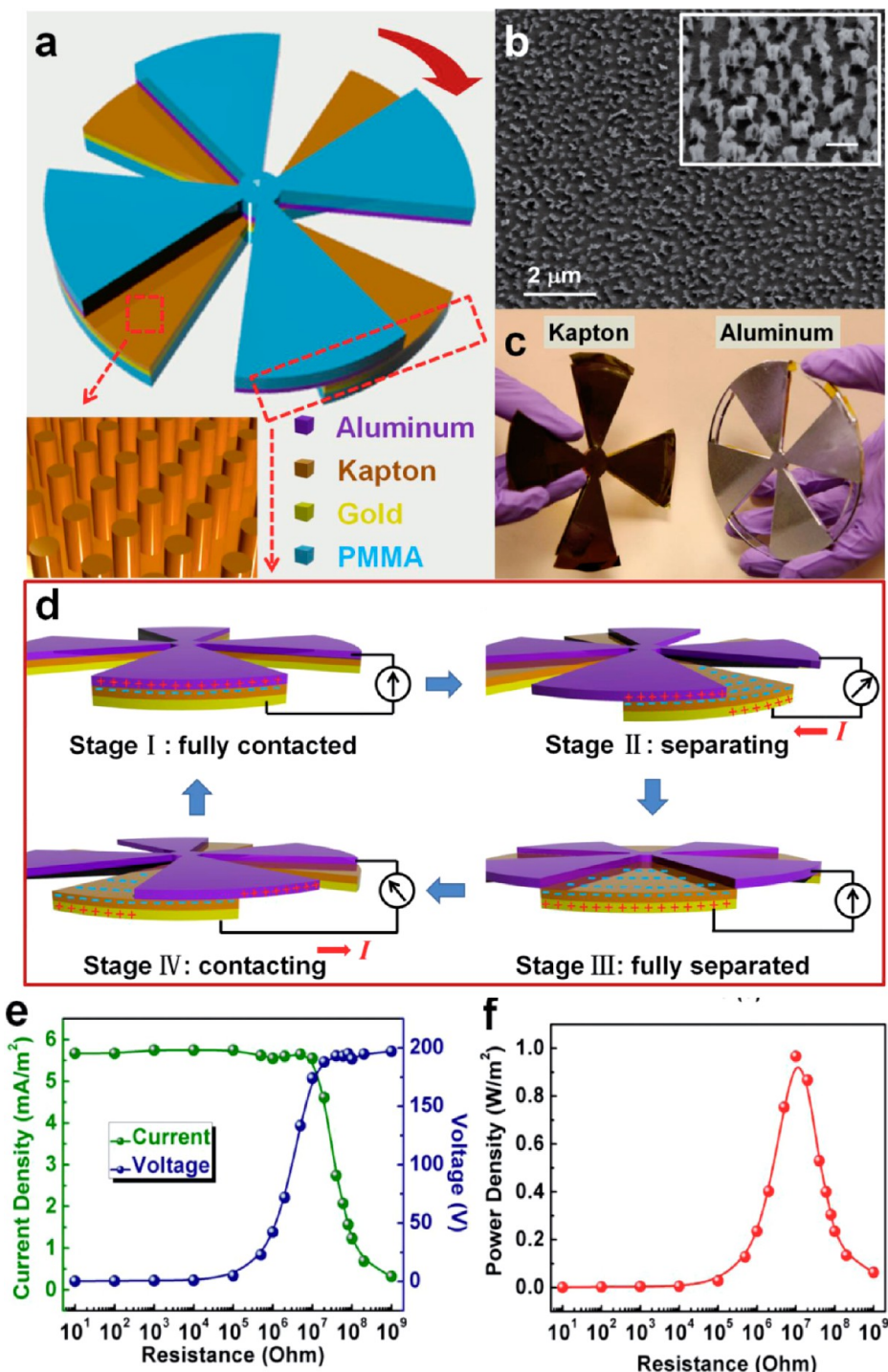


**Figure 10.** Rotating TENG in segmented disk configuration. (a) Schematic illustration showing the structure design of the disk TENG. The inset (bottom left) is an enlarged figure showing the Kapton nanorod array created on the surface area. (b) Top view SEM image of the Kapton nanorods showing its uniformity in a large range. The inset is a high-magnification SEM image of the Kapton nanorods in 30° tilted view. The scale bar is 500 nm. (c) Photograph showing the two parts of a real disk TENG. (d) Schematic illustrations showing the proposed working principle of the disk TENG with the electron flow diagram in four consecutive stages within a full cycle of electricity generation. Please note that only one pair of sectors (the cross-section area entangled in Figure 1a was shown with surface charges for clarity of illustration, and the surface charges on the interface area between Al foil and Kapton film are hidden and are not drawn for easy presentation. (e) relationship between the output voltage/current and the resistance of an external load. (f) Relationship between the effective power density and the resistance of the external load. The maximum power is received when the external resistance is  $10 \text{ M}\Omega$ . Reproduced from ref 27. Copyright 2013 American Chemical Society.

created by the separated tribo-charges. In this process, the electrons keep flowing until the two disks are fully

mismatch in the contacting segmented areas (e.g., for 45° rotation in this case), which is represented by stage

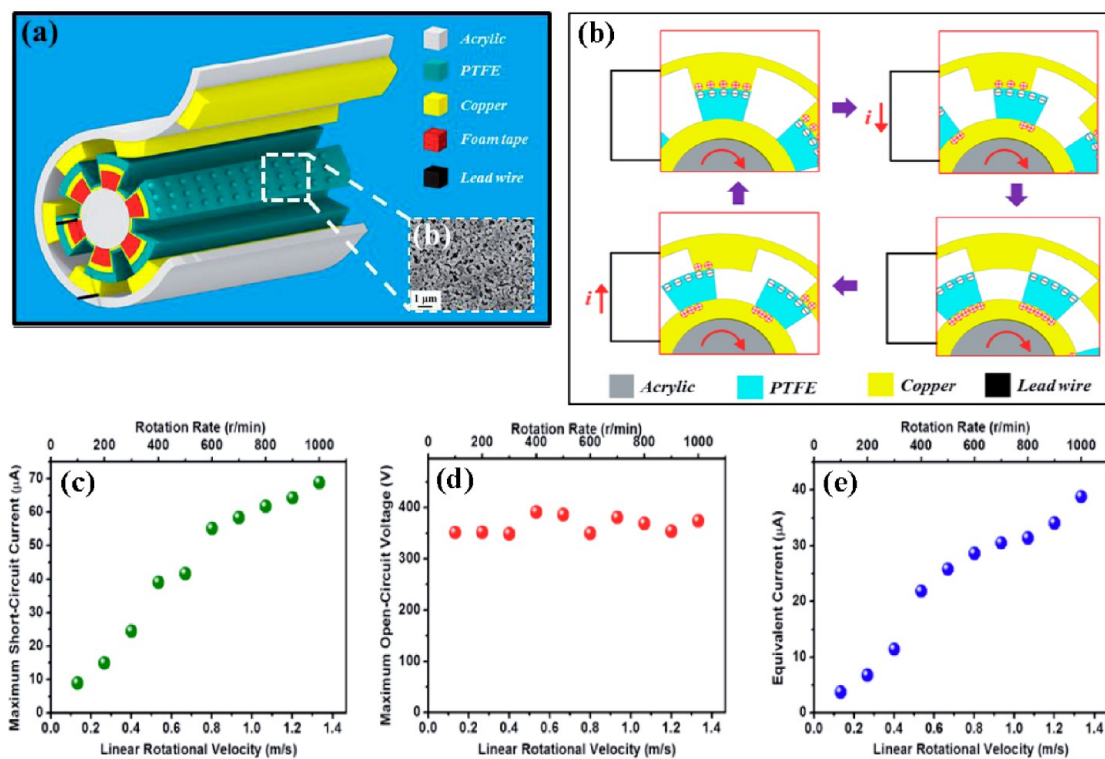


**Figure 11.** Rotation TENG in cylindrical configuration. (a) Design and structure of the cylindrical rotation TENG. (b) Working principle of the TENG. (c) Maximum  $I_{sc}$  as a function of linear rotational velocity/rotation rate of 1.33 m/s (a rotation rate of 1000 r/min). (d) Maximum  $V_{oc}$  as a function of linear rotational velocity/rotation rate. (e) Equivalent direct current as a function of linear rotational velocity/rotation rate. Reproduced from ref 28. Copyright 2013 American Chemical Society.

III. At this moment, both the induced potential difference and the amount of transferred charges between the two electrodes reach the maximum values. In stage IV, as the top plate continues spinning, the Kapton surface begins to contact another adjacent sector of Al foil, and the potential difference between two electrodes will drop with the decrease of the mismatch area. As a result, the electrons will flow back in the opposite direction from the Al foil to the electrode attached to the Kapton film. Thus, the entire process will result in an alternating current (AC) output. Such a charge transfer cycle will start over from stage I when the two plates reach a complete overlapping again. Figure 10e shows the resistance dependence of both output current density and voltage, from  $10\ \Omega$  to  $1\ G\Omega$ . The output current density decreases with the increasing resistance, while the output voltage shows the reverse trend, but both the current and voltage tend to saturate at both high and low ends of the resistance. The power density was also plotted as a function of external resistance in Figure 10f. The output power density first increases at a low resistance region and then decreases at a higher resistance region. The maximum value of the power density of  $\sim 1\ W/m^2$  occurs at  $\sim 10\ M\Omega$ .

A schematic diagram of a cylindrical rotating TENG with 6 strip units is shown in Figure 11a.<sup>28</sup> The TENG has a core–shell structure that is composed of a

column connected to a rotational motor and a hollow tube fixed on a holder. Here, acrylic was selected as the structural material due to its light weight, good machinability, and proper strength. On the inner surface of the fixed tube, metal strips made of copper are evenly distributed, with each having a central angle of  $30^\circ$ , creating equal-sized intervals between. These metal strips, connected by a bus at one end, play dual roles as a sliding surface and as a common electrode. On the surface of the rotatable column, a collection of separated strips of foam tape were adhered as a buffer layer with a central angle of  $30^\circ$  for each unit. The buffer layer is a critical design that ensures robustness and tolerance on off-axis rotation, which will be discussed in detail later. On top of the foam tape, a layer of copper and a layer of PTFE film are conformably attached in sequence. The copper layer serves as back electrode of the TENG. The outer surface of the PTFE film is modified by spreading a layer of PTFE nanoparticles to enhance energy conversion efficiency.

The working principle of a rotating TENG can be described by the coupling of contact electrification and electrostatic induction. The design of the cylindrical rotating TENG is based on the relative sliding motion of grated surfaces. Here, a pair of sliding units is selected to illustrate the process of electricity generation, as schemed in Figure 11b. The foam tape and nanoparticles on the PTFE film are not presented for

simplification and clear illustration. At the aligned position, the two parts of the sliding pair completely match because of the same central angle. Upon contact between the PTFE film and the metal strips, charge transfer takes place. Due to the difference on triboelectric polarities, electrons are injected from metal into the surface of PTFE. Since the two sliding surfaces are completely aligned, triboelectric charges with opposite polarities are fully balanced out, making no electron flow in the external circuit (Figure 11bI). Once a relative sliding occurs as a result of rotation, triboelectric charges on the mismatched areas cannot be compensated. The negative ones on the PTFE will drive free electrons on the back electrode to the sliding electrode through the external circuit due to electrostatic induction, neutralizing positive triboelectric charges on the sliding electrode and leaving positively induced charges behind on the back electrode (Figure 11bII). The flow of the induced electrons lasts until the mismatch between the two sliding surfaces reaches the maximum when the positive triboelectric charges are fully screened by induced electrons (Figure 11bIII). As the relative rotation continues, the PTFE film will come into contact with an adjacent metal strip (Figure 11bIV). Thus, the induced electrons will flow back in an opposite direction until the fully aligned position is restored (Figure 11bI). Therefore, in a cycle of electricity generation, AC electric output is generated. Since all of the sliding units are electrically connected in parallel, output current from different units are synchronized to constructively add up.

To characterize the electric output,  $I_{sc}$  and  $V_{oc}$  of a rotating TENG with 6 strip units were measured at a rotation rate of 1000 r/min, corresponding to an equivalent linear rotational velocity of 1.33 m/s. An approximately linear relationship between the linear rotational velocity and the current amplitude can be derived from the results shown in Figure 11c. The linear relationship between the velocity and output current can be explained by the increasing frequency. The  $V_{oc}$  stays stable at different rotation rate because the voltage is only a function of percentage of mismatch as shown in Figure 11d. For output charge, a higher current frequency produces a larger amount of accumulative charges within the same period of time, resulting in a larger equivalent direct current. As shown in Figure 11e, the equivalent direct current increases from 3.7 to 38.9  $\mu$ A when the linear rotational velocity increases from 0.13 to 1.33 m/s.

**Single-Electrode-Based TENG.** The TENGs presented in the last few sections must have two electrodes in order to form a closed circuit for the electrons to flow. Such a configuration is possible for a working alone system, but it introduces difficulty in engineering design for specific applications such as harvesting energy from a rotating tire. In this section, we introduce a single-electrode-based TENG that is more practical and

feasible design for some applications such as finger-tip-driven TENG.<sup>29–32</sup> To obtain a more quantitative understanding about the TENG, we employed finite element simulation to calculate the electric potential distribution in the TENG and the charge transfer between the ITO electrode and ground using COMSOL. The constructed model is based on a skin patch and a PDMS film on the ITO electrode with the dimensions of 45 mm × 65 mm and thickness of 1 mm for skin, 0.5 mm for PDMS film, 1 mm for ITO electrode, as depicted in Figure 12a. The ITO electrode was connected with the ground. The triboelectric charge densities on the skin and PDMS film were assumed to be +10 and  $-10 \mu$ C/m<sup>2</sup>, respectively. Figure 12b shows the calculated results of the electric potential distribution in the TENG under the different separation distances of 0.5, 10, 30, and 60 mm. When the skin and PDMS fully contact with each other, the electric potentials on both the skin and PDMS approach zero. The electric potential difference was found to increase dramatically with increasing separation distance. When they are separated by 60 mm, the electric potential on the skin surface reaches  $1.2 \times 10^4$  V, while the electric potential on the PDMS is still close to zero, which is associated with contact with the ITO electrode/ground. As illustrated in Figure 12c, the amount of the total charges on the ITO electrode was plotted as a function of separation distance between the skin and PDMS. It increases with increasing separation distance, revealing that charge transfer decreases with increasing distance. These results are consistent with the measured change in charge quantity when the contacted skin was removed from the PDMS film, as shown in Figure 12d.

The working principle of the fabricated TENG is schematically shown in Figure 12e by the coupling of contact electrification and electrostatic induction. In the original position, the surfaces of skin and PDMS fully contact with each other, resulting in charge transfer between them. According to the triboelectric series, electrons were injected from the skin to the PDMS since the PDMS is more triboelectrically negative than skin, which is the contact electrification process. The produced triboelectric charges with opposite polarities are fully balanced/screened, leading to no electron flow in the external circuit. Once a relative separation between PDMS and skin occurs, these triboelectric charges cannot be compensated. The negative charges on the surface of the PDMS can induce positive charges on the ITO electrode, driving free electrons to flow from the ITO electrode to ground. This electrostatic induction process can give an output voltage/current signal if the distance separating the touching skin and the bottom PDMS is appreciably comparable to the size of the PDMS film. When negative triboelectric charges on the PDMS are fully screened from the induced positive charges on the ITO electrode by increasing the

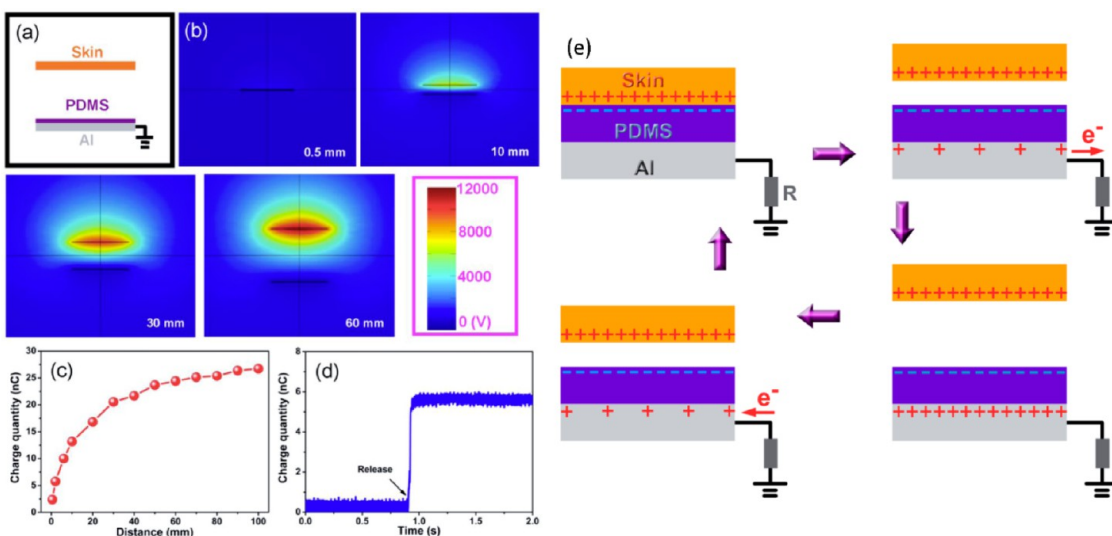


**Figure 12.** Single-electrode TENG in contact-separation mode. (a) Schematic diagram of the model for the calculation. (b) Finite element simulation of the potential distribution in the TENG for the different separation distances between the skin and PDMS film. (c) Total charges on the ITO electrode as a function of the separation distance between the skin and PDMS film. The increase in total charges is a result of the electron flow from ITO to ground. (d) Measured charge quantity when the applied pressure on the PDMS film was released. (e) Sketches that illustrate the electricity generation process in a full cycle. (I) Full contact between the human skin and PDMS film. (II) Two surfaces are separated with a small distance. (III) Two surfaces are separated with a large distance. (IV) Separated two surfaces are approaching. Reproduced with permission from ref 29. Copyright 2013 Wiley.

separation distance between the PDMS and skin, no output signals can be observed, as illustrated. Moreover, when the skin was reverted to approach the PDMS, the induced positive charges on the ITO electrode decrease and the electrons will flow from ground to the ITO electrode until the skin and PDMS fully contact with each other again, resulting in a reversed output voltage/current signal. This is a full cycle of the electricity generation process for the TENG in contact-separation mode.

The mechanism of the single-electrode-based sliding TENG is schematically depicted in Figure 13a. In the original position, the surfaces of PTFE and Al fully overlap and intimately contact with each other. According to the triboelectric series, the contact between the PTFE and Al will result in electrons being injected from Al to PTFE since PTFE is much more triboelectrically negative than Al. The produced negative triboelectric charges can be preserved on the PTFE surface for a long time due to the nature of the insulator. Once the top PTFE with the negatively charged surface starts to slide outward, it will result in the decrease of the induced positive charges on the Al, thus the electrons flow from ground to Al, producing a positive current signal. When the top PTFE fully slides out of the bottom Al, the two triboelectric charged surfaces are entirely separated, and then an equilibrium state can be created with no output voltage/current. When the top PTFE plate is reverted to slide backward, the induced positive charges on the Al increase, driving the electrons to flow from Al to ground to produce a negative current signal. Once the two plates completely reach

the overlapping position, the charged surfaces get into full contact again and there will be no change of the induced charges on the Al, thus no output current can be observed. This is a full cycle of the single-electrode-based sliding TENG working process.

The electric potential distribution in the TENG and the charge transfer between the Al and ground can be verified through numerical simulation using COMSOL. The proposed model is based on a PTFE patch and an Al plate with the same dimensions ( $5\text{ cm} \times 8\text{ cm} \times 0.1\text{ cm}$ ), as shown in the inset of Figure 13b. The triboelectric charge density on the PTFE was assumed to be  $-10\text{ }\mu\text{C/m}^2$ . The Al plate was connected with the ground. Figure 13b depicts the calculated results of the electric potential distribution in the TENG under four different sliding distances of 0, 16, 26, and 40 mm. When two plates are fully overlapped, the electric potential on the PTFE surface approaches zero. When the top PTFE plate slides out with a displacement of 26 mm, the electric potential on the PTFE surface is up to  $-6000\text{ V}$ . It can be clearly seen that the electric potential difference between the PTFE and the Al increases dramatically with increasing sliding distance. As illustrated in Figure 13c, the amount of the total charges on the Al plate decreases linearly with increasing sliding distance, indicating that the transferred charges between Al and the ground increase with the increasing sliding distance.

Usually, the effective output power of the TENG depends on the match with the loading resistance. Figure 13d shows the resistance dependence of both output voltage and the output current density with the

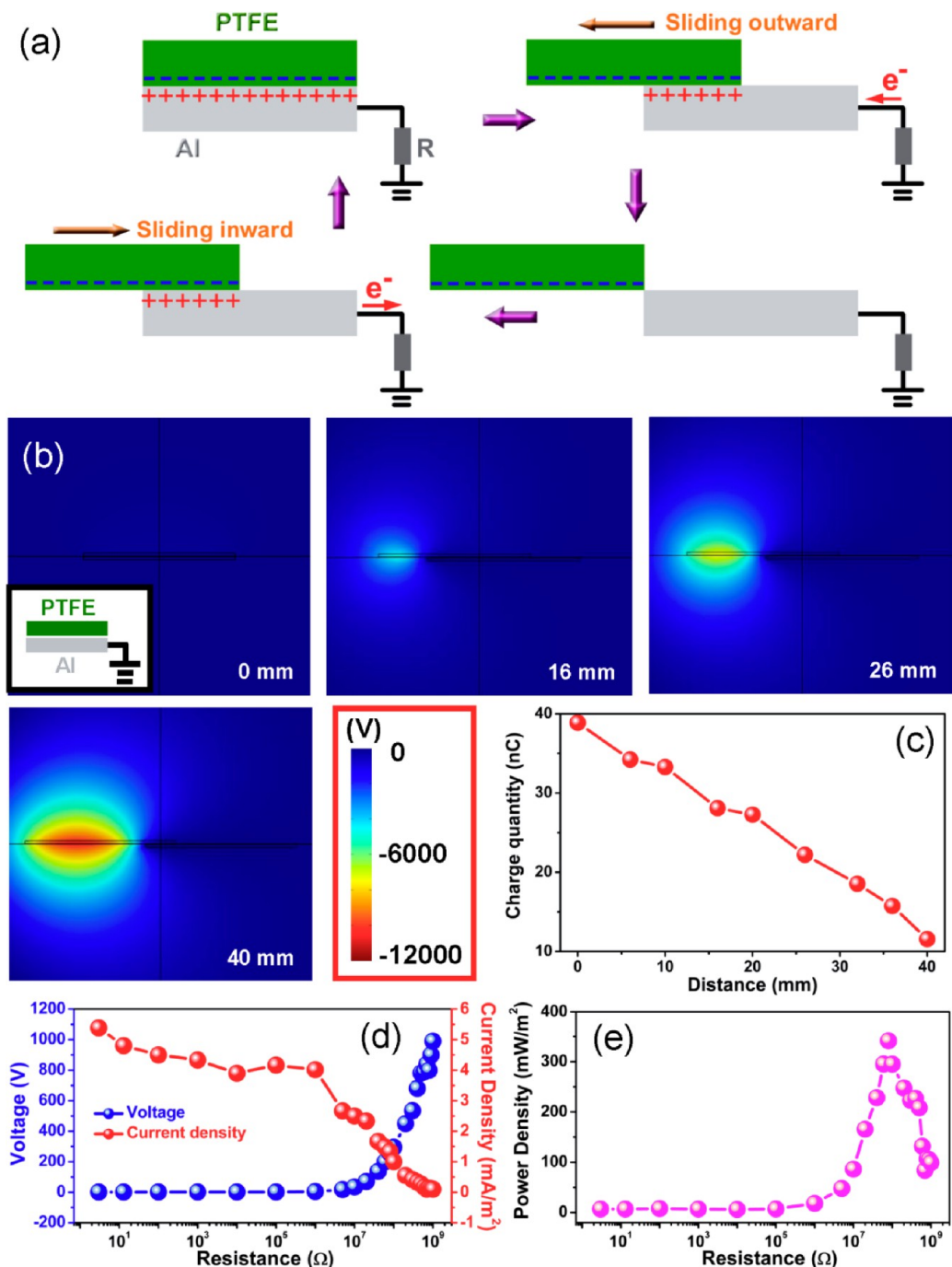


**Figure 13.** Single-electrode TENG in sliding mode. (a) Sketches that illustrate the electricity generation process in a full cycle. (b) Finite element simulation of the potential distribution in the TENG. The inset shows the model for the calculation with the separation distance of 0.2 mm between PTFE and Al. (c) Curve of the induced charge quantity on the Al electrode *versus* the sliding distance from 0 to 40 mm. (d) Dependence of the output voltage and the current density on the external loading resistance. (e) Plot of the power density *versus* the loading resistance. Reproduced from ref 30. Copyright 2013 American Chemical Society.

resistance from  $10 \Omega$  to  $1 \text{ G}\Omega$ . The output voltage of the device rises up with increasing the loading resistance, while the current density drops with the increase of the resistance. As shown in Figure 13e, the output power density was plotted as a function of the loading resistance. The instantaneous power density remains close to 0 with the resistance below  $1 \text{ M}\Omega$  and then increases in the resistance region from 1 to  $100 \text{ M}\Omega$ .

The power density decreases under the larger loading resistance ( $>100 \text{ M}\Omega$ ). The maximum value of the output power density reaches  $350 \text{ mW}/\text{m}^2$  at a loading resistance of  $100 \text{ M}\Omega$ .

**Applications of TENG.** TENG is a physical process of converting mechanical agitation to an electric signal through the triboelectrification (in inner circuit) and electrostatic induction processes (in outer circuit).

This basic process has been demonstrated for two major applications. The first application is energy harvesting with a particular advantage of harvesting mechanical energy. The other application is to serve as a self-powered active sensor because it does not need an external power source to drive. In this section, we briefly summarize the applications that have been demonstrated in these two areas.

**Harvesting Vibration Energy.** Vibration is one of the most popular phenomena in our daily life, from walking, voices, engine vibration, automobile, train, aircraft, wind, and many more. It exists almost everywhere and at all times. Harvesting vibration energy is of great value especially for powering mobile electronics. Based on the fundamental principles introduced in section 4, various technologies have been demonstrated for harvesting vibration energy.

Cantilever-based technique is a classical approach for harvesting mechanical energy, especially for MEMS. By designing the contact surface of a cantilever with the top and bottom surfaces during vibration, TENG has been demonstrated for harvesting ambient vibration energy based on the contact-separation mode. With the assistance of nanowire arrays fabricated onto the surfaces of beryllium copper alloys foils, the newly designed TENG produces an open-circuit voltage up to 101 V, a short-circuit current of  $55.7 \mu\text{A}$ , with a corresponding peak power density of  $252.3 \text{ mW/m}^2$ .<sup>33</sup>

To harvest the energy from a backpack, we demonstrated a rationally designed TENG with integrated rhombic gridding, which greatly improved the total current output owing to the structurally multiplied unit cells connected in parallel.<sup>34</sup> With the hybridization of both the contact-separation mode and sliding electrification mode among nanowire arrays and nanopores fabricated onto the surfaces of two contact plates, the newly designed TENG produces an open-circuit voltage up to 428 V and a short-circuit current of 1.395 mA with a peak power density of  $30.7 \text{ W/m}^2$ . Based on the TENG, a self-powered backpack was developed with a vibration-to-electric energy conversion efficiency up to 10.6%. The newly designed TENG can be a mobile power source for field engineers, explorers, and disaster-relief workers.

With the use of four supporting springs, a harmonic resonator-based TENG has been fabricated based on the resonance-induced contact separation between the two triboelectric materials, which has been used to harvest vibration energy from an automobile engine, a sofa, and a desk.<sup>35</sup> It produces a uniform quasi-sinusoidal signal output, with an open-circuit voltage up to 287.4 V, a short-circuit current amplitude of  $76.8 \mu\text{A}$ , and a peak power density  $726.1 \text{ mW/m}^2$ . It can effectively respond to input vibration frequency from 2 to 200 Hz with a considerably wide working bandwidth of 13.4 Hz. The harmonic resonator-based TENG is very sensitive to small ambient vibrations such as an

operating automobile engine; it can also act as an active vibration sensor for ambient vibration detection. This work not only presents a new principle in the field of vibration energy harvesting but also greatly expands the applicability of TENGs as power sources for self-sustained electronics.

Recently, a three-dimensional triboelectric nano-generator (3D-TENG) has been designed based on a hybridization mode of conjunction the vertical contact-separation mode and the in-plane sliding mode.<sup>36</sup> The innovative design facilitates harvesting random vibration energy in multiple directions over a wide bandwidth. An analytical model is established to investigate the mechano-triboelectric transduction of 3D-TENG, and the results agree well with experimental data. Compared with the state-of-the-art vibration energy harvesters, the 3D-TENG is able to harvest ambient vibration in out-of-plane direction (z-axis) with extremely wide working bandwidth up to 75 Hz at a frequency of  $\sim 63.5 \text{ Hz}$  ( $\Delta f/f \sim 1.18$ ) and arbitrary in-plane (x–y plane) directions with a bandwidth of 14.4 Hz at a frequency of  $\sim 38 \text{ Hz}$  ( $\Delta f/f \sim 0.38$ ). The maximum power densities of 1.35 and  $1.45 \text{ W/m}^2$  have been achieved under out-of-plane and in-plane excitations, respectively. The 3D-TENG is designed for harvesting ambient vibration energy, especially at low frequencies, under a range of conditions in daily life, thus, opening the applications of TENG in environmental/infrastructure monitoring, charging portable electronics, and Internet.

**Harvesting Energy from Human Body Motion.** Human motion has an abundant amount of energy, which can be useful for charging portable electronics and biomedical applications. We have demonstrated a packaged power-generating insole with built-in flexible multilayered triboelectric nanogenerators that enable harvesting mechanical pressure during normal walking. The TENG used here relies on the contact-separation mode and is effective in responding to the periodic compression of the insole. Using the insole as a direct power source, we develop a fully packaged self-lighting shoe that has broad applications for display and entertainment purposes. Furthermore, a prototype of a wearable charging gadget is introduced to charge portable consumer electronics, such as cell phones. This work presents a successful initial attempt in applying energy-harvesting technology for self-powered electronics in our daily life, which will have broad impact on people's living style in the near future.

A TENG can be attached to the inner layer of a shirt for harvesting energy from body motion. Under general walking, the maximum output of voltage and current density are up to 17 V and  $0.02 \mu\text{A/cm}^2$ , respectively. The TENG with a single layer size of  $2 \text{ cm} \times 7 \text{ cm} \times 0.08 \text{ cm}$  sticking on clothes was demonstrated as a sustainable power source that not only can directly light up 30 light-emitting diodes but

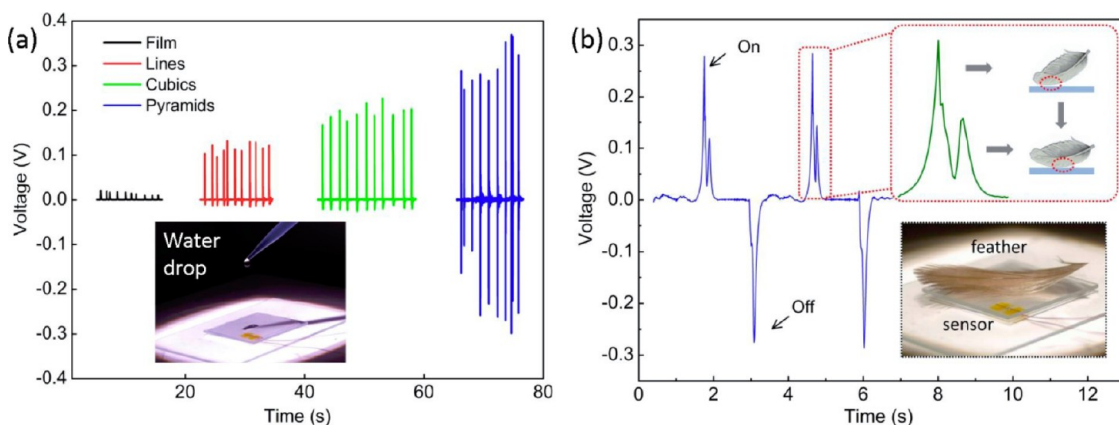


**Figure 14.** TENG as self-powered pressure sensor. (A) Performance of the pressure sensor device induced by a droplet of water falling from about 5 cm high. The voltage responses of various types of sensor devices were measured. (B) Performance of the pressure sensor device induced by a piece of feather. The top inset image illustrates the process that a double peak was induced by placement of the feather. The bottom inset image shows the photograph of the feather induced pressure sensor. Reproduced from ref 15. Copyright 2012 American Chemical Society.

also can charge a lithium ion battery by persistently clapping clothes. The electric energy stored in the lithium ion battery was used to power a biosensor for detecting glucose. The detection of bioactive chemicals in our body using the energy harvested from body motion is demonstrated. Moreover, due to the sensitivity and desirable stability to periodic vibration, the TENG was used to measure stride frequency, as well.

**TENG as Self-Powered Active Strain/Force Sensors.** A TENG automatically generates an output voltage and current once it is mechanically triggered. The magnitude or the output signal signifies the impact of the mechanical deformation and its time-dependent behavior. This basic principle of the TENG can be applied as a self-powered pressure sensor.<sup>15,37,38</sup> Figure 14a illustrates the voltage output signal of various types of sensor devices to the applied pressure induced by a droplet of water (8 mg, ~3.6 Pa of pressure). All types of TENGs have a high sensitivity and fast response to the external force and show a sharp peak signal. The sensitivities of the line-featured and cube-featured sensors were about 5 and 10 times, respectively, larger than that of the unstructured film-featured sensor. The pyramid-featured device showed the highest sensitivity in the four types of pressure sensors. Furthermore, we measured the response to the impact of a piece of feather (20 mg, ~0.4 Pa in contact pressure), corresponding to a low-end detection limit of 13 mPa. In Figure 14b, the sensor shows two opposite voltage signal curves indicating the feather loading (on) and unloading (off) process. In the real situation, when the feather falls on the sensor, it will go through two processes: initially touching the sensor and completely falling on the sensor. The sensor signal can delicately show these details of the entire process. The existing results show that our sensor can be applied to measure the subtle pressure in real life.

In the case where we make a matrix array of TENGs, we can have a large-area and self-powered pressure map applied on a surface.<sup>32</sup> The response of the TENG array with local pressure was measured through a multichannel measurement system. On the basis of this working principle, we demonstrated the tactile imaging capability of the TEAS matrix by loading pressure through predesigned plastic architecture with the calligraphy of the letters "TENG". Before applying the pressure, the voltage output from all of the pixels of the TEAS matrix was at the background level, as displayed in Figure 15b. Figure 15c–f shows the two-dimensional contour plot of the peak value of the voltage responses that were measured when external pressures were applied through each architecture. The highlighted color represents the area under pressing through each letter, as outlined by the white dashed lines. These plots elaborate the spatial resolution of the TEAS matrix for distinguishably mapping the calligraphy of the applied pressure and its potential applications such as personal signature recognition. In addition, to gain a more intuitive understanding of the "self-powered" pressure mapping functionality of the TEAS matrix, each nine units of the same array device were connected in parallel to power up a serially connected array of LEDs showing "T", "E", "N", and "G". This demonstration proves that the TEAS matrix can work as an external power source and a sensor array simultaneously for a truly stand-alone self-powered system.

There are two types of output signals from the TENG: open-circuit voltage and short-circuit current. The open-circuit voltage is only dictated by the final configuration of the TENG after applying a mechanical triggering, so that it is a measure of the magnitude of the deformation, which is attributed to the static information to be provided by TENG. The output current depends on the rate at which the induced

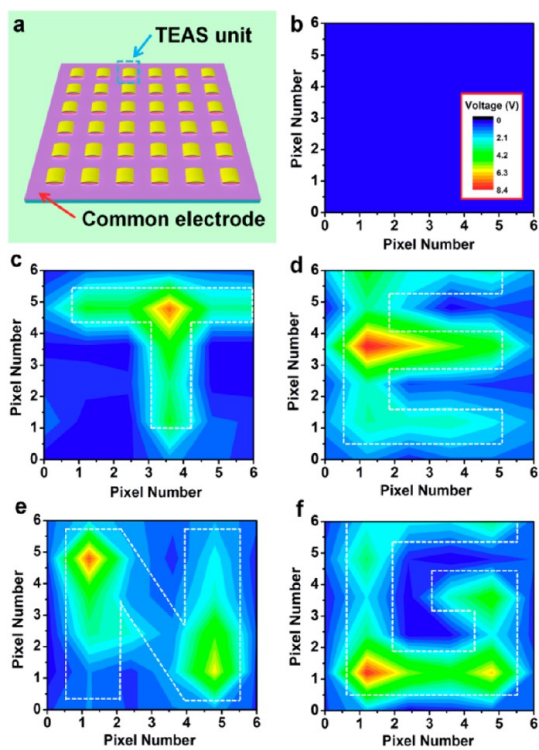


**Figure 15.** Self-powered pressure mapping using an array of TENG. (a) Schematic illustration of the TENG array. (b) Background signal with no pressure applied on the TENG matrix. The inset is color scaling of voltage for all the measurements in this figure. (c–f) Two-dimensional voltage contour plot from the multichannel measurement of the TENG matrix with an external pressure uniformly and locally applied onto the device through architectures with calligraphy of “T”, “E”, “N”, and “G”. Reproduced from ref 37. Copyright 2013 American Chemical Society.

charge would flow, so that the current signal is more sensitive to the dynamic process of how the mechanical triggering is applied.

The active pressure sensor and the integrated sensor array based on the triboelectric effect presented in this work have several advantages over conventional passive pressure sensors. First, the active sensor in this work is capable of both static pressure sensing using the open-circuit voltage and dynamic pressure sensing using the short-circuit current, while conventional sensors are usually incapable of dynamic sensing to provide the loading rate information. Second, the prompt response of both static and dynamic sensing enables the revealing of details about the loading pressure. Third, the detection limit of the TENG for dynamic sensing is as low as 2.1 Pa, owing to the high output of the TENG. Fourth, the active sensor array presented in this work has no power consumption and could even be combined with its energy harvesting functionality for self-powered pressure mapping. Future works in this field involve the miniaturization of the pixel size to achieve higher spatial resolution, and the integration of the TEAS matrix onto a fully flexible substrate for shape-adaptive pressure imaging.

One of the materials for the TENG can be human skin based on the single-electrode-based TENG.<sup>30</sup> This allows a direct interface of fingertip and a transparent bottom electrode material as device for touch pad and smart skin applications. As shown in Figure 16, the output voltage signals of 16 devices were recorded in real-time as a mapping figure. By addressing and monitoring the positive output voltage signals in 16 channels of the tactile sensor system, the touched information of a human finger including the position and pressure can be attained by analysis of the measured mapping figures. If larger pressure is applied on the device, the larger output voltage signals can be observed in the mapping figures. Figure 16a presents a photograph of the device when the sixth and 11th devices in the matrix were simultaneously touched. Two, almost the same, pressures of about 4.9 kPa can be confirmed by the analysis of the obtained same output voltage signals in the corresponding mapping image, as shown in Figure 16b. Figure 16c displays the response of the device to the localized pressure induced by two fingers when the matrix was rotated by 90°. The obtained mapping figure clearly reveals that the seventh and 10th devices were touched, where the produced pressures of about 7.0 kPa are larger than those in Figure 16b. When the pressures were applied along the diagonal line of the matrix by using the side surface of a human hand, the distinctive changes in the output voltage signals can be observed, revealing an increase of the pressure from 3.2 to 6.0 kPa along the diagonal line, as illustrated in Figure 16d. When the pressures were applied on all 16 devices by using the human hand, the recorded mapping figure (Figure 16e) shows that all the devices are functional and the pressures on devices 1–8 are obviously larger than those on devices 9–16. The real-time detection of the touched actions on the flexible devices is a desirable feature for sensors embedded in robots or prosthetic devices. Figure 16f shows a photograph of the flexible matrix attached to a transparent acrylic tube. When the pressures were applied on the tube surface by using the human hand, the largest pressure of about 7.3 kPa occurs at the marked area (the white dashed line in Figure 16g), which is consistent with the measured mapping figure, as shown in Figure 16k. Such a demonstration can also be done by placing a transparent TENG array on the display panel of a cell phone or underneath the keyboards during typing, clearly demonstrating its potential as sensors and as potential energy harvester.

**TENG as Self-Powered Active Chemical Sensors.** As for TENG, maximizing the charge generation on opposite sides can be achieved by selecting the materials with the largest difference in the ability to attract electrons and changing the surface morphology. In such a case, the output of the TENG depends on the type and concentration of molecules adsorbed on the

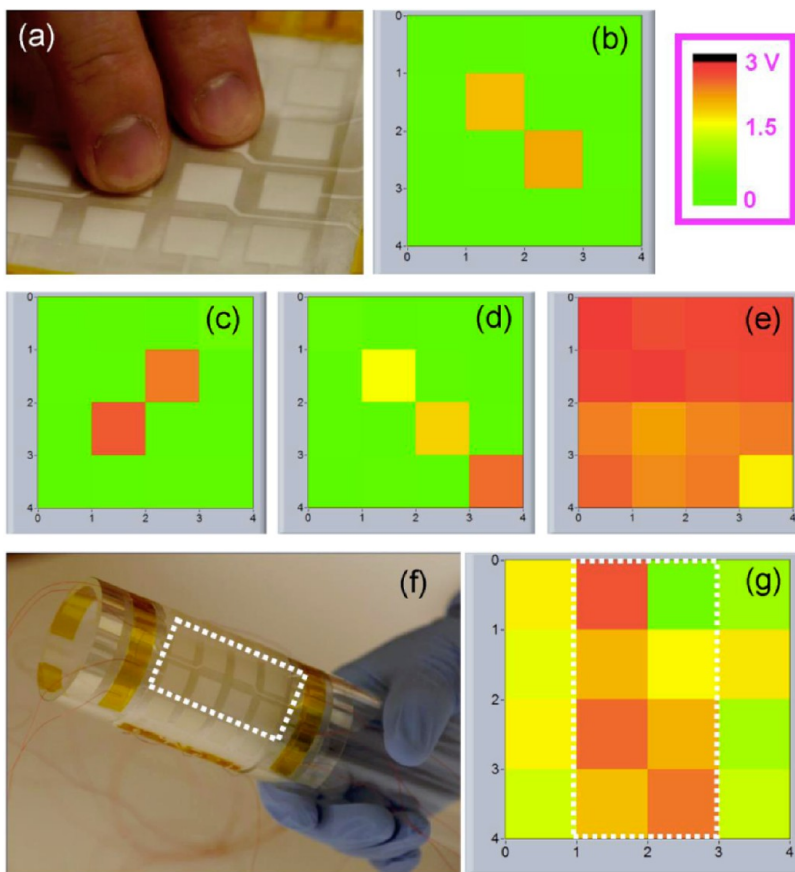


**Figure 16.** TENG as self-powered touch pad sensor and smart skin. (a) Photograph of the matrix touched by two human fingers. (b–e) Measured mapping figures under different pressures. (f) Photograph of the fabricated matrix attached to an acrylic tube. (g) Measured mapping figure when the device in (f) was touched by a human hand. Reproduced from ref 31. Copyright 2013 American Chemical Society.

surface of the triboelectric materials, which can be used for fabricating chemical and biochemical sensors.<sup>39</sup> In our case, the performance of the TENG depends on the assembly of Au nanoparticles (NPs) onto the metal plate. These assembled Au NPs not only act as steady gaps between the two plates at strain-free conditions but also enable the function of enlarging the contact area of the two plates, which will increase the electrical output of the TENG. Through further modification of 3-mercaptopropionic acid (3-MPA) molecules on the assembled Au NPs, the high-output nanogenerator can become a highly sensitive and selective nanosensor toward  $\text{Hg}^{2+}$  ion detection because of the different triboelectric polarity of Au NPs and  $\text{Hg}^{2+}$  ions (Figure 17a). On the basis of this unique structure, the output voltage and current of the triboelectric nanosensor (TENG) reached 105 V and 63  $\mu\text{A}$  with an effective dimension of  $1 \text{ cm} \times 1 \text{ cm}$ . Under optimum conditions, this TENG is selective for the detection of  $\text{Hg}^{2+}$  ions, with a detection limit of 30 nM and linear range from 100 nM to 5  $\mu\text{M}$  (Figure 17b). With its high sensitivity, selectivity, and simplicity, the TENG holds great potential for the determination of  $\text{Hg}^{2+}$  ions in environmental samples. The TENG is a future sensing system for unreachable and access-denied

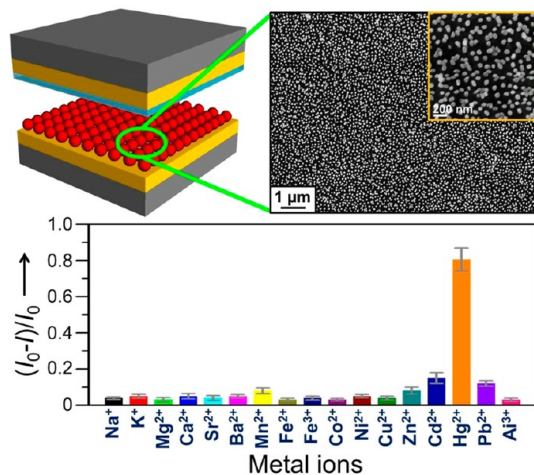


**Figure 17.** TENG as self-powered chemical sensor for detecting  $\text{Hg}^{2+}$  ions. Top: Fabrication of the TENG functionalized with Au nanoparticles at one side. Bottom: Sensitivity and selectivity of the as-developed TENG for the detection of  $\text{Hg}^{2+}$  ions. The concentration of all metal ions tested in the selectivity experiment was 5  $\mu\text{M}$ . Reproduced with permission from ref 39. Copyright 2013 Wiley.

extreme environments. As different ions, molecules, and materials have their unique triboelectric polarities, we expect that the TENG can become either an

**TABLE 1. Triboelectric Series for Some Common Materials Following a Tendency To Easily Lose Electrons (Positive) and To Gain Electrons (Negative)<sup>6</sup>**

 <b>Positive</b>	Polyformaldehyde 1.3-1.4	(continued)	 <b>Negative</b>
	Etylcellulose	Polyester (Dacron)	
	Polyamide 11	Polyisobutylene	
	Polyamide 6-6	Polyurethane flexible sponge	
	Melanime formol	Polyethylene Terephthalate	
	Wool, knitted	Polyvinyl butyral	
	Silk, woven	Polychlorobutadiene	
	Aluminum	Natural rubber	
	paper	Polyacrylonitrile	
	Cotton, woven	Acrylonitrile-vinyl chloride	
	Steel	Polybisphenol carbonate	
	Wood	Polychloroether	
	Hard rubber	Polyvinylidene chloride (Saran)	
	Nickel, copper	Polystyrene	
	Sulfur	Polyethylene	
	Brass, silver	Polypropylene	
	Acetate, Rayon	Polyimide (Kapton)	
	Polymethyl methacrylate (Lucite)	Polyvinyl Chloride (PVC)	
	Polyvinyl alcohol	Polydimethylsiloxane (PDMS)	
	(continued)	Polytetrafluoroethylene (Teflon)	
 <b>Positive</b>	Aniline-formol resin	Polyvinyl alcohol	 <b>Negative</b>
	Polyformaldehyde 1.3-1.4	Polyester (Dacron) (PET)	
	Etylcellulose	Polyisobutylene	
	Polyamide 11	Polyurethane flexible sponge	
	Polyamide 6-6	Polyethylene terephthalate	
	Melanime formol	Polyvinyl butyral	
	Wool, knitted	Formo-phenolique, hardened	
	Silk, woven	Polychlorobutadiene	
	Polyethylene glycol succinate	Butadiene-acrylonitrile copolymer	
	Cellulose	Nature rubber	
	Cellulose acetate	Polyacrylonitrile	
	Polyethylene glycol adipate	Acrylonitrile-vinyl chloride	
	Polydiallyl phthalate	Polybisphenol carbonate	
	Cellulose (regenerated) sponge	Polychloroether	
	Cotton, woven	Polyvinylidene chloride (Saran)	
	Polyurethane elastomer	Poly(2,6-dimethyl polyphenyleneoxide)	
	Styrene-acrylonitrile copolymer	Polystyrene	
	Styrene-butadiene copolymer	Polyethylene	
	Wood	Polypropylene	
	Hard rubber	Polydiphenyl propane carbonate	
	Acetate, Rayon	Polyimide (Kapton)	
	Polymethyl methacrylate (Lucite)	Polyethylene terephthalate	
	Polyvinyl alcohol	Polyvinyl Chloride (PVC)	
	(continued)	Polytrifluorochloroethylene	
		Polytetrafluoroethylene (Teflon)	

electrical turn-on or turn-off sensor when the analytes are selectively binding to the modified electrode surface. We believe this work will serve as the stepping stone for related TENG studies and inspire the development of TENG toward other metal ions and biomolecules such as DNA and proteins in the near future.

**Water-Surface-Based TENG for Chemical Sensors.** Most recently, we have demonstrated a newly designed TENG based on the contact electrification between a patterned PDMS pyramid array and water.<sup>40</sup> This new prototype water-TENG provided an open-circuit voltage of 52 V and a short-circuit current density of 2.45 mA m<sup>-2</sup> with a peak power density of nearly 0.13 W m<sup>-2</sup>. The dependence of the electrical outputs on the contact frequency and motions of water wave has been systematically studied. Tap water and deionized water with similar ion concentration to seawater were also evaluated and showed the potential for harvesting water-related energy from the environment. Compared with traditional TENGs that are designed for the contact of solid materials, this study opens the possibility of utilizing liquid movements and extends its application scope in chemistry and chemical sensors.

**Theory of TENG.** To help understand the basic output of the TENG, analytical and numerical theories have been developed to calculate the output voltage, current, and charges.<sup>41</sup> A theoretical model for the contact-separation mode TENG was first developed. Based on the theoretical model, its real-time output characteristics and the relationship between the optimum resistance and TENG parameters were derived. The theory can serve as an important guidance for rational design of the TENG structure in specific applications.

A theoretical model for the sliding-mode TENG has also been developed. The finite element method was utilized to characterize the distributions of electric potential, electric field, and charges on the metal electrodes of the TENG.<sup>42</sup> Based on the FEM calculation, the semianalytical results from the interpolation method and the analytical  $V$ – $Q$ – $x$  relationship were built to study the sliding-mode TENG. The analytical  $V$ – $Q$ – $x$  equation was validated through comparison with the semianalytical results. Furthermore, based on the analytical  $V$ – $Q$ – $x$  equation, dynamic output performance of sliding-mode TENG was calculated with arbitrary load resistance, and good agreement with experimental data was reached. The theory presented here is a milestone work for in-depth understanding of the working mechanism of the sliding-mode TENG and provides a theoretical basis for further enhancement of the sliding-mode TENG for both energy scavenging and self-powered sensor applications.

**Choice of Materials and Surface Structures.** Almost all materials we know have triboelectrification effect, from metal, to polymer, to silk, and to wood, almost everything. All of these materials can be candidates for

fabricating TENGs, so the material choices for TENGs are huge. However, the ability of a material to gain/lose electrons depends on its polarity. John Carl Wilcke published the first triboelectric series in 1757 on static charges.<sup>43,44</sup> Table 1 gives such a series for some conventional materials. A material toward the bottom of the series, when touched to a material near the top of the series, will attain a more negative charge. The further away two materials are from each other on the series, the greater the charge transferred.

Beside the choice of the materials in the triboelectric series, the morphologies of the surfaces can be modified by physical techniques with the creation of pyramid-, square-, or hemisphere-based micro- or nanopatterns, which are effective for enhancing the contact area and possibly the triboelectrification. However, the created bumpy structure on the surface may increase the friction force, which may possibly reduce the energy conversion efficiency of the TENG. Therefore, an optimization has to be designed to maximize the conversion efficiency.

The surfaces of the materials can be functionalized chemically using various molecules, nanotubes, nanowires, or nanoparticles, in order to enhance the triboelectrification effect. Surface functionalization can largely change the surface potential. The introduction of nanostructures on the surfaces can change the local contact characteristics, which may improve the triboelectrification. This will involve a large amount of studies for testing a range of materials and a range of available nanostructures.

Besides these pure materials, the contact materials can be made of composites, such as embedding nanoparticles in a polymer matrix. This changes not only the surface electrification but also the permittivity of the materials so that they can be effective for electrostatic induction.

Therefore, there are numerous ways to enhance the performance of the TENG from the materials point of view. This gives an excellent opportunity for chemists and materials scientists to do extensive study both in basic science and in practical applications. In contrast, materials systems for solar cell and thermal electrics, for example, are rather limited, and there are not very many choices for high-performance devices.

## SUMMARY AND PERSPECTIVES

As sparked by the first discovery of nanogenerators in 2006, research in nanoenergy has inspired worldwide interest. Nanoenergy is about the applications of nanomaterials and nanotechnology for harvesting energy for powering micro/nanosystems. The discovery of the triboelectric nanogenerator (TENG) is a major milestone in the field of converting mechanical energy into electricity for building self-powered systems. It offers a completely new approach for harvesting mechanical energy using organic and inorganic materials.

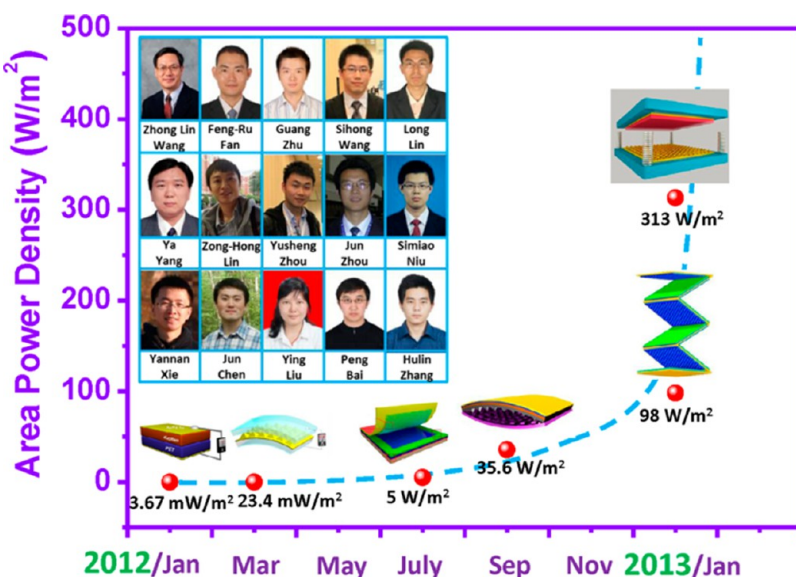


**Figure 18.** Summary on the progress made in the output power density of a TENG within 12 months. The insets are the people in Wang's group who have made important contributions to the discovery and development of TENG.

Figure 18 gives a summary about our progress made from January 2012 to January 2013 in the performance of the TENG, a 5 order of magnitude enhancement in output power density! The area power density reaches  $313 \text{ W/m}^2$ , and volume density reaches  $490 \text{ kW/m}^3$ . The TENG can be made into multilayers so that we have a three-dimensional nanogenerator. Such high performance outplays many existing technologies in its category. We anticipate that much more enhancement of the output power density will be demonstrated in the next few years. Such a huge output makes it possible not only for self-powered portable electronics but also for harvesting energy from wind and ocean wave. Therefore, TENG is a new energy technology for the next century! We anticipate a worldwide study of TENG in the next few years, and soon some industrial products and applications will be achieved. Since the mostly useful materials are organic, TENG is an organic nanogenerator, which is expected to be equally important as organic LEDs and organic solar cells.

Furthermore, TENG has to be hybridized with other technologies such as solar cell and thermal electric generators to simultaneously harvest multiple-type energies. TENG also has to be hybridized with an energy storage unit to form a self-charged power pack. The future is about material and device hybridization. The self-powering idea is a new paradigm in nanotechnology for truly achieving sustainable self-sufficient micro/nanosystems, which are of critical importance for sensing, medical science, infrastructure/environmental monitoring, defense technology, and even personal electronics. Therefore, nano is not only beautiful but, more importantly, nano has to be useful! Nanotechnology has the obligation to solve some of the critical problems facing the sustainable

development of the world. This has to be the goal of nanotechnology now and in the future.

*Conflict of Interest:* The authors declare no competing financial interest.

*Acknowledgment.* Research was supported by BES DOE, NSF, Airforce, Samsung, SKKU (Korea), MANA NIMS (Japan), and the Knowledge Innovation Program of the Chinese Academy of Sciences (KJCX2-YW-M13). I thank my group members and my collaborators for their contributions to the work reviewed here. Thanks to Dr. Yong Ding for his assistance in the preparation of the manuscript. All of the materials presented have been published and proper references have been cited, and some published figures and possibly text have been used for this review article.

*Note Added after ASAP Publication:* This paper published ASAP on October 3, 2013. Figures 6 and 7 were adjusted to correct a figure/caption mismatch and the revised version was reposted on October 14, 2013.

## REFERENCES AND NOTES

1. Wang, Z. L.; Song, J. H. Piezoelectric Nanogenerators Based on Zinc Oxide Nanowire Arrays. *Science* **2006**, *312*, 242–246.
2. Wang, Z. L. Nanogenerators for Self-Powered Devices and Systems. Georgia Institute of Technology, 2011.
3. Wang, Z. L. ZnO Nanowire and Nanobelt Platform for Nanotechnology. *Mater. Sci. Eng. R* **2009**, *64*, 33–71.
4. Wang, Z. L.; Yang, R. S.; Zhou, J.; Qin, Y.; Xu, C.; Hu, Y. F.; Xu, S. Lateral Nanowire/Nanobelt Based Nanogenerators, Piezotronics and Piezo-Phototronics. *Mater. Sci. Eng. R* **2010**, *70*, 320–329.
5. Henniker, J. Triboelectricity in Polymers. *Nature* **1962**, *196*, 474.
6. Davies, D. K. Charge Generation on Dielectric Surfaces. *J. Phys. D: Appl. Phys.* **1969**, *2*, 1533–1537.
7. Wang, Z. L.; Wu, W. Z. Nanotechnology-Enabled Energy Harvesting for Self-Powered Micro-/Nanosystems. *Angew. Chem., Int. Ed.* **2012**, *51*, 11700–11721.
8. Elsdon, R.; Mitchell, F. R. G. Contact Electrification of Polymers. *J. Phys. D: Appl. Phys.* **1976**, *9*, 1445–1460.
9. McCarty, L. S.; Whitesides, G. M. Electrostatic Charging Due to Separation of Ions at Interfaces: Contact Electrification of Ionic Electrets. *Angew. Chem., Int. Ed.* **2008**, *47*, 2188–2207.

10. Cole, J. J.; Barry, C. R.; Knuesel, R. J.; Wang, X. Y.; Jacobs, H. O. Nanocontact Electrification: Patterned Surface Charges Affecting Adhesion, Transfer, and Printing. *Langmuir* **2011**, *27*, 7321–7329.
11. Baytekin, H. T.; Baytekin, B.; Soh, S.; Grzybowski, B. A. Is Water Necessary for Contact Electrification? *Angew. Chem., Int. Ed.* **2011**, *50*, 6766–6770.
12. Baytekin, H. T.; Patashinski, A. Z.; Branicki, M.; Baytekin, B.; Soh, S.; Grzybowski, B. A. The Mosaic of Surface Charge in Contact Electrification. *Science* **2011**, *333*, 308–312.
13. Zhou, Y. S.; Liu, Y.; Zhu, G.; Lin, Z. H.; Pan, C. F.; Jing, Q. S.; Wang, Z. L. In Situ Quantitative Study of Nanoscale Triboelectrification and Patterning. *Nano Lett.* **2013**, *13*, 2771–2776.
14. Fan, F. R.; Tian, Z. Q.; Wang, Z. L. Flexible Triboelectric Generator!. *Nano Energy* **2012**, *1*, 328–334.
15. Fan, F. R.; Lin, L.; Zhu, G.; Wu, W. Z.; Zhang, R.; Wang, Z. L. Transparent Triboelectric Nanogenerators and Self-Powered Pressure Sensors Based on Micropatterned Plastic Films. *Nano Lett.* **2012**, *12*, 3109–3114.
16. Zhu, G.; Pan, C. F.; Guo, W. X.; Chen, C. Y.; Zhou, Y. S.; Yu, R. M.; Wang, Z. L. Triboelectric-Generator-Driven Pulse Electrodeposition for Micropatterning. *Nano Lett.* **2012**, *12*, 4960–4965.
17. <http://www.trifield.com/content/tribo-electric-series/>.
18. Diaz, A. F.; Felix-Navarro, R. M. A Semi-quantitative Triboelectric Series for Polymeric Materials: The Influence of Chemical Structure and Properties. *J. Electrostat.* **2004**, *62*, 277–290.
19. Wang, S. H.; Lin, L.; Wang, Z. L. Nanoscale Triboelectric-Effect-Enabled Energy Conversion for Sustainably Powering Portable Electronics. *Nano Lett.* **2012**, *12*, 6339–6346.
20. Zhu, G.; Lin, Z. H.; Jing, Q. S.; Bai, P.; Pan, C. F.; Yang, Y.; Zhou, Y. S.; Wang, Z. L. Toward Large-Scale Energy Harvesting by a Nanoparticle-Enhanced Triboelectric Nanogenerator. *Nano Lett.* **2013**, *13*, 847–853.
21. Zhong, J. W.; Zhong, Q. Z.; Fan, F. R.; Zhang, Y.; Wang, S. H.; Hu, B.; Wang, Z. L.; Zhou, J. Finger Typing Driven Triboelectric Nanogenerator and Its Use for Instantaneously Lighting up LEDs. *Nano Energy* **2013**, *2*, 491–497.
22. O'Donnell, R.; Schofield, N.; Smith, A. C.; Cullen, J. Design Concepts for High-Voltage Variable-Capacitance DC Generators. *IEEE Ind. Appl.* **2009**, *45*, 1778–1784.
23. Bai, P.; Zhu, G.; Lin, Z. H.; Jing, Q. S.; Chen, J.; Zhang, G.; Ma, J.; Wang, Z. L. Integrated Multilayered Triboelectric Nanogenerator for Harvesting Biomechanical Energy from Human Motions. *ACS Nano* **2013**, *7*, 3713–3719.
24. Zhang, X. S.; Han, M. D.; Wang, R. X.; Zhu, F. Y.; Li, Z. H.; Wang, W.; Zhang, H. X. Frequency-Multiplication High-Output Triboelectric Nanogenerator for Sustainably Powering Biomedical Microsystems. *Nano Lett.* **2013**, *13*, 1168–1172.
25. Zhu, G.; Chen, J.; Liu, Y.; Bai, P.; Zhou, Y. S.; Jing, Q. S.; Pan, C. F.; Wang, Z. L. Linear-Grating Triboelectric Generator Based on Sliding Electrification. *Nano Lett.* **2013**, *13*, 2282–2289.
26. Wang, S. H.; Lin, L.; Xie, Y. N.; Jing, Q. S.; Niu, S. M.; Wang, Z. L. Sliding-Triboelectric Nanogenerators Based on In-Plane Charge-Separation Mechanism. *Nano Lett.* **2013**, *13*, 2226–2233.
27. Lin, L.; Wang, S. H.; Xie, Y. N.; Jing, Q. S.; Niu, S. M.; Hu, Y. F.; Wang, Z. L. Segmentally Structured Disk Triboelectric Nanogenerator for Harvesting Rotational Mechanical Energy. *Nano Lett.* **2013**, *13*, 2916–2923.
28. Bai, P.; Zhu, G.; Liu, Y.; Chen, J.; Jing, Q. S.; Yang, W. Q.; Ma, J. S.; Zhang, G.; Wang, Z. L. Cylindrical Rotating Triboelectric Nanogenerator. *ACS Nano* **2013**, *7*, 6261–6266.
29. Yang, Y.; Zhou, Y. S.; Zhang, H. L.; Chen, J.; Liu, Y.; Lee, S. M.; Wang, Z. L. Single-Electrode Based Triboelectric Nanogenerator as Self-Powered Tracking System. *Adv. Mater.* **2013** in press.
30. Yang, Y.; Zhang, H. L.; Chen, J.; Jing, Q. S.; Zhou, Y. S.; Wen, X. N.; Wang, Z. L. Single-Electrode-Based Sliding Triboelectric Nanogenerator for Self-Powered Displacement Vector Sensor System. *ACS Nano* **2013**, *7*, 7342–7351.
31. Yang, Y.; Zhang, H. L.; Lin, Z. H.; Zhou, Y. S.; Jing, Q. S.; Su, Y. J.; Yang, J.; Chen, J.; Hu, C. G.; Wang, Z. L. Human Skin Based Triboelectric Nanogenerators for Harvesting Biomechanical Energy and as Self-Powered Active Tactile Sensor System. *ACS Nano* **2013**, *10*.1021/nn403838y.
32. Meng, B.; Tang, W.; Too, Z. H.; Zhang, X. S.; Han, M. D.; Liu, W.; Zhang, H. X. A Transparent Single-Friction-Surface Triboelectric Generator and Self-Powered Touch Sensor. *Energy Environ. Sci.* **2013**, *10*.1039/C3EE42311E.
33. Yang, W. Q.; Chen, J.; Zhu, G.; Wen, X. N.; Bai, P.; Su, Y. J.; Lin, Y. F.; Wang, Z. L. Harvesting Vibration Energy by a Triple-Cantilever Based Triboelectric Nanogenerator. *Nano Res.* **2013**, *10*.1007/s12274-013-0365-z.
34. Yang, W. Q.; Chen, J.; Zhu, G.; Yang, J.; Bai, P.; Su, Y. J.; Jing, Q. S.; Wang, Z. L. Harvesting Energy from Natural Vibration of a Human Walking. *Energy Environ. Sci.* **2013** in press.
35. Chen, J.; Zhu, G.; Yang, W. Q.; Jing, Q. S.; Bai, P.; Su, Y. J.; Lin, Y.; Wang, Z. L. Harmonic Resonator Based Triboelectric Nanogenerator as Sustainable Power Source and Self-Powered Active Vibration Sensor. *Adv. Mater.* **2013**, *10*.1002/adma.201302397.
36. Yang, J.; Yang, Y.; Chen, J.; Zhang, H. L.; Yang, W. Q.; Bai, P.; Su, Y. J.; Wang, Z. L. Broadband Vibration Energy Harvesting Based on Triboelectric Nanogenerator. *Adv. Energy Mater.* **2013** submitted.
37. Lin, L.; Xie, Y. N.; Wang, S. H.; Wu, W. Z.; Niu, S. M.; Wen, X. N.; Wang, Z. L. Triboelectric Active Sensor Array for Self-Powered Static and Dynamic Pressure Detection and Tactile Imaging. *ACS Nano* **2013**, *7*, 8266–8274.
38. Zhang, H. L.; Yang, Y.; Su, Y. J.; Chen, J.; Adams, K.; Lee, S. M.; Hu, C. G.; Wang, Z. L. Triboelectric Nanogenerator for Harvesting Vibration Energy in Full Space and as Self-Powered Acceleration Sensor. *Adv. Funct. Mater.* **2013** in press.
39. Lin, Z. H.; Zhu, G.; Zhou, Y. S.; Yang, Y.; Bai, P.; Chen, J.; Wang, Z. L. A Self-Powered Triboelectric Nanosensor for Mercury Ion Detection. *Angew. Chem., Int. Ed.* **2013**, *52*, 5065–5069.
40. Lin, Z. H.; Cheng, G.; Lin, L.; Lee, S. M.; Wang, Z. L. Water-Solid-Surface Contact Electrification and Its Use for Harvesting Liquid Wavy Energy. *Angew. Chem., Int. Ed.* **2013**, *10*.1002/anie.201307249.
41. Niu, S. M.; Wang, S. H.; Lin, L.; Liu, Y.; Zhou, Y. S.; Hu, Y. F.; Wang, Z. L. Theoretical Study of the Contact-Mode Triboelectric Nanogenerators as Effective Power Source. *Energy Environ. Sci.* in press.
42. Niu, S. M.; Liu, Y.; Wang, S. H.; Lin, L.; Zhou, Y. S.; Hu, Y. F.; Wang, Z. L. Theory of Sliding-mode Triboelectric Nanogenerators. *Adv. Mater.*, DOI: *10.1002/adma.201302808*.
43. <http://owlsmag.wordpress.com/2010/01/20/a-natural-history-devin-corbin/>.
44. Disputatio Physica Experimentalis, De Electricitatibus Contrariis. Typis Ioannis Iacobi Adleri, **1757**.